Modeling of Growth and Electrical Properties of Phosphorus Doped n-Si Microneedle Grown by Vapor-Liquid-Solid Method

A thesis submitted in partial fulfillment of the requirements for the degree of

Master of Science

In

Electrical and Electronic Engineering

By

Nurunnahar Islam Mou

Under the supervision of

Dr. Md. Shofiqul Islam

Department of Electrical and Electronic Engineering

BANGLADESH UNIVERSITY OF ENGINEERING AND TECHNOLOGY

July 2012

Approval

The thesis titled **"Modeling of Growth and Electrical Properties of Phosphorus Doped n-Si Microneedle Grown by Vapor-Liquid-Solid Method"** submitted by Nurunnahar Islam Mou, Student No: 1009062061, Session: October, 2009, has been accepted as satisfactory in partial fulfillment of the requirement for the degree of MASTER OF SCIENCE IN ELECTRICAL AND ELECTRONIC ENGINEERING on July 11, 2012.

BOARD OF EXAMINERS

1.____

Dr. Md. Shofiqul Islam
Associate Professor
Department of Electrical and Electronic Engineering,
Bangladesh University of Engineering and Technology (BUET),
Dhaka – 1000, Bangladesh.

Chairman
(Supervisor)

2.____

Dr. Pran Kanai Saha
Professor and Head
Department of Electrical and Electronic Engineering,
Bangladesh University of Engineering and Technology (BUET)
Dhaka – 1000, Bangladesh

Member
(Ex-officio)

3.____

Dr. Md. Nasim Ahmed Dewan
Associate Professor
Department of Electrical and Electronic Engineering, BUET
Dhaka – 1000, Bangladesh.

Member

4.____

Dr. Md. Anwarul Abedin
Professor
Dept of EEE, DUET
Gazipur

Member
(External)

Candidate's declaration

It is hereby declared that this thesis work is the outcome of the original work of the undersigned student. This thesis or any part of it has not been submitted elsewhere for the award of any degree or diploma and that all sources are acknowledged.

Signature of the Candidate

____

(Nurunnahar Islam Mou)

Student No. :1009062061F

Dedication

TO MY PARENTS AND SISTER

Acknowledgement

First of all, I would like to thank Allah for giving me the ability to complete this thesis work.

I would like to express my sincere and heartfelt gratitude to all those who lent me a hand to complete this thesis work. Firstly, I would like to thank the Department of Electrical And Electronic Engineering, BUET, for giving me permission to commence this thesis in the first instance, to do the necessary research work and to use the Departmental facilities.

I am deeply indebted to my supervisor Dr. Md. Shofiqul Islam (Associate Professor, Department of Electrical and Electronic Engineering, BUET, Bangladesh) for his guidance in my research work. He has steered me successfully to achieve the research objective with his knowledge, experience and stimulating suggestions. Furthermore, I would like to thank Dr. Saifur Rahman (Professor, Department of Electrical and Electronic Engineering, BUET, Bangladesh) for his kind help.

Special thanks go to Mr. Kamrul Hasan, my senior friend from the Department of Electrical and Electronic Engineering (EEE), BUET for his support in conducting my research. I would also like to thank my dear friend Nitu Syed from the Department of Electrical and Electronic Engineering, BUET for great help and support for conducting my research work.

I would like to take this opportunity to give special thanks to the authority of Independent University, Bangladesh for giving their support and providing me printing, photocopying and internet use facilities for this thesis work.

Finally, I would like to thank my family members for their unconditional love and support in all situations which made me stronger and determined. Last but not the least; I must convey my earnest thanks to all of my friends for their continuous support and encouragement.

Abstract

Semiconducting microstructures and nanostructures are promising candidates in MEMs, optoelectronics, sensor circuits and photovoltaics. Needle like Si microstructures have found several novel applications. Si microneedles can be fabricated in many ways, however, the Vapor Liquid Solid (VLS) process is one of the most prominent method for fabricating needle like crystals directly.

Highly conductive doped Si microneedles are required for sensing small signals and for device fabrication. By *in situ* doping into VLS growth mechanism, more conductive needles can be grown. Phosphorus doped n-type silicon microneedles have been grown via *in situ* doping VLS method using gold (Au) as catalyst particle with disilane (Si_2H_6) as Si precursor source and phosphine (PH_3) as the dopant source. Experimental data shows that the doping changes the growth kinetics and electrical properties of the needles. Thus phosphorus doping brings about new challenges such as control of sizes, structures, and properties of microneedles during the synthesis step. Hence the purpose of this thesis work was to study and analyze the physical and electrical characteristics of phosphorus doped Si microneedles in detail with proper mathematical modeling.

At the very first, the effect of changing doping level on the growth rate has been analyzed. A mathematical model relating growth rate with doping level was derived which is compatible with the experimental result. Similarly the effect of microneedle diameter on the growth rate has been explained with mathematical relation based on the experimental data and related research works. Again the dependency of the diameter of the needle on doping level and other initial conditions of VLS growth was analyzed and explained in this work. At last the electrical characteristics of phosphorus doped Si microneedle was investigated and explained using the physics of metal-semiconductor junction, Schottky barrier and band theory. All the results of this work have been compared with experimental data to justify the compatibility of the models.

The mathematical model and analysis in this thesis will be very helpful to anticipate the size of such phosphorus doped microneedles and hence to fabricate microneedles of desired length and diameter for certain applications. The analysis of the electrical properties will also be helpful to improve the I-V characteristics in future while fabricating vertical devices like diodes, transistors with Si microneedles.

List of contents

APPROVAL..ii

DECLARATION..iii

DEDICATION..iv

ACKNOWLEDGEMENT..v

ABSTRACT..vi

LIST OF TABLES xi

LIST OF FIGURES..xii

1. INTRODUCTION 1

1.1. Scope of the thesis..1

1.2. State of the problem..1

1.3. Objectives..2

1.4. Approach..3

1.5. Organization of the thesis..4

2. MICRONEEDLE FABRICATION 6

2.1. Introduction..6

2.2. Review of previous work..7

2.3. Fabrication process..8

2.3.1. Chemical vapor deposition (CVD)..8

2.3.2. Annealing in reactive atmosphere..10

2.3.3. Evaporation of SiO..10

2.3.4. Molecular beam epitaxy (MBE)..11

2.3.5. Laser ablation..11

2.3.6. Solution based techniques....12
2.3.7. Top-down fabrication process....13
2.4. Application of microneedles....14
2.4.1. Force and temperature sensors....14
2.4.2. Biotechnology....15
2.4.3. Medical science....15
2.4.4. On-chip devices....16
2.4.5. Photovoltaics....17
2.5. Vapor-liquid-solid mechanism....18
2.5.1. Introduction....18
2.5.2. Fundamentals of VLS mechanism....18
2.5.3. VLS growth process....20
2.5.3.1. Alloying process....20
2.5.3.2. Nucleation process....21
2.5.3.3. Axial growth....22
2.6. *In situ* doped VLS....22
2.6.1. n-Si microneedle fabrication....22
2.6.2. Results....24
2.7. Conclusion....25
3. GROWTH RATE ANALYSIS 26
3.1. Introduction....26
3.2. Effect of phosphorus doping on microneedle growth....26
3.2.1. Experimental findings....27
3.2.2. Theoretical analysis....27
3.2.3. Mathematical modeling....28

3.3. The effect of droplet size on microneedle growth....32
3.3.1. Experimental findings....32
3.3.2. Fundamental of crystal growth....33
3.3.3. Growth rate dependency on Au dot diameter....35
3.3.3.1. Considering only direct adsorption....35
3.3.3.2. Considering only diffusion of adsorbent....40
3.3.3.3. Combining both effects....42
3.4. Conclusion....42
4. DIAMETER ANALYSIS 43
4.1. Introduction....43
4.2. Effect of Au dot size on microneedle diameter....43
4.2.1. Experimental findings....43
4.2.2. Theoretical analysis....45
4.2.3. Mathematical relation....45
4.3. Effect of doping on microneedle diameter....47
4.3.1. Experimental findings....48
4.3.2. Theoretical analysis....49
4.4. Conclusion....51
5. I-V CHARACTERISTICS ANALYSIS 53
5.1. Introduction....53
5.1.1. Experimental findings....53
5.2. I-V analysis....54
5.2.1. Metal n-type semiconductor contact....55
5.2.2. J-V equation....56

5.2.3. Simulation result....59

5.2.4. Comparison between experimental and simulation result....59

5.3. Conclusion....60

6. CONCLUSION AND FUTURE WORK 62

6.1. Summary....62

6.2. Scope of future research work....63

REFERENCES....65

List of Tables

2.1 Experimental data of phosphorus doped n-Si microneedle growth.........................25

3.1 Growth rate variation of n-Si microneedle from experimental data with various flow of PH_3 at a temperature of 720° C, at a growth pressure of $5x10^{-3}$ Pa and disilane (Si_2H_6) flow rate of 1.7 sccm..27

3.2 Growth rate variation of n-Si microneedle as a function of flow rate of PH_3 calculated from the proposed model and from experimental values........................31

3.3 Growth rate for different Au-dot size..33

4.1 Microneedle diameter for different Au dot size..45

4.2 Experimental data for microneedle diameter for doping level................................48

5.1 I-V characteristics data of n-Si microneedle with a length of 52µm and a diameter of 2.8µm for PH_3 flow rate of 0.15sccm 54

5.2 Table comparing Experimental and simulated data for I-V characteristic...............61

List of figures

2.1 Si microneedle grown on Si substrate by VLS method..7

2.2 Schematics of experimental setups for silicon wire growth a) CVD, b) annealing in reactive atmosphere, c) evaporation of SiO, d) MBE, e) laser ablation, and f) solution-based growth...9

2.3 Out-of-plane silicon microwire-based artificial whisker array sensor by selective VLS growth of p-silicon on n-silicon...14

2.4 Microneedle electrode grown by dry etching inserted into cells for intracellular recording..15

2.5 A pointed single crystal silicon needle..16

2.6 SEM views of Si probes grown by selective VLS growth using a Au catalyst and SiH gas. The VLS growth realizes micro-Si probes with a Au–Si alloy dot at the tip and a single crystalline Si body...16

2.7 Schematics of conventional p-channel MOSFET and a silicon nanowire vertical surround-gate field-effect-transistor grown by VLS method..................................17

2.8 Photograph of a six-inch wafer covered in Si microwires (left) and SEM image of these wires (right)...17

2.9 Three basic stages of VLS mechanism...18

2.10 Schematic illustration of the VLS process, Si_2H_6 molecules in the vapor phase are flown over metal catalyst particles on a substrate. These molecules decompose preferentially at the catalyst to form a liquid droplet if the sample is held near or above the eutectic temperature. Lastly, a solid single crystal is extruded from the liquid melt...20

2.11 Binary Au-Si phase diagram...21

2.12 Silicon microneedles grown by Vapor-Liquid-Solid mechanism............................22

2.13 Fabrication process of n-Si microprobe array: (a) SiO_2 layer formation; (b) circular window through SiO_2 made by photolithography; (c) Au film deposition; (d) lift-off Au from resist-site; (e) annealing to form Au-Si alloy droplet; (f) introduction of mixed gas of PH_3 and Si_2H_6 into the growth chamber and then n-Si microprobes grow by VLS mechanism..23

2.14 SEM image of n-Si microprobe array with probe-length of 54μm and probe-diameter of 3.6 μm, which were grown by *in situ* doping VLS with PH_3 = 1.00 sccm and Si_2H_6 = 1.70 sccm..24

3.1 Growth rate variation of n-Si microneedle with various flow of PH_3.......................27

3.2 Dependence of growth rate of Si probe and that of poly-Si on temperature. Both Si probe and poly-Si..30

3.3 Growth rate variation of n-Si microneedle as a function of PH_3 flow rate calculated from proposed model..30

3.4 Comparison of growth rate variation of n-Si microneedle as a function of doping level from the proposed growth rate model and from experimental data, grown by VLS at a temperature 720°C and at the growth pressure $5x10^{-3}$Pa..........................31

3.5 Growth rate (μm/min) vs. Au dot size (μm) for various PH_3 flow rate....................33

3.6 Experimentally grown phosphorus doped Si microneedle.......................................35

3.7 Top: Scanning electron micrographs indicating the development of the droplet shape in the initial phase of growth. Center: Schematic development of droplet and wire shape in the initial phase of growth. Bottom: the corresponding equilibrium balance of surface forces at the left edge of the droplet (dashed circles). Note: horizontal force components add up to zero...36

3.8 (a) Au-Si alloy droplet on Si microneedle (β>90°) (b) spherical coordinate system 37

3.9 Scanning electron micrographs of GaP nanowires grown with MOVPE at different temperatures: (A) 440°C (B) 470°C and (C) 500°C...40

3.10 Contribution of diffusion in needle growth..41

4.1 Experimental results of microneedle diameter as a function of Au dot size for PH_3 flow rate (a) 0.15sccm (b) 0.5sccm...44

4.2 Theoretical relation between Microneedle diameter and Au dot diameter..............47

4.3 Microneedle diameter vs. doping level...48

4.4 Contact angle (measured in gas phase) as a function of temperature.......................49

4.5 Vectorial equilibrium for a droplet of a liquid resting on a solid.............................50

5.1 I-V characteristics curve of n-Si microneedle with a length of 52μm and a diameter of 2.8μm for PH_3 flow rate of 0.15sccm...53

5.2 SEM image of n-Si microneedle array grown by *in situ* doped VLS.......................55

5.3 Band diagram of metal-n-ype semiconductor ohmic contact...................................55

5.4 I-V characteristics of metal-semiconductor contact for different doping conditions 56

5.5 Theoretical and experimental current-voltage characteristics for Au-Si Schottky barriers. Increased current is due to tunneling...57

5.6 I-V characteristics curve of n-Si microneedle from Atlas simulator (for low doping level)..59

5.7 I-V characteristics curve of n-Si microneedle from Atlas simulator (for high doping level)..60

5.8 I-V comparison between the simulated data and experimental data.........................60

CHAPTER 1

INTRODUCTION

1.1 Scope of the thesis

Semiconducting microstructures and nanostructures are promising candidates in MEMs, optoelectronics, sensor circuits and photovoltaics. Needle like Si microstructures have found several applications like Si needles as the pins for developing high-resolution probe card for IC testing [1], needle-like Si-microprobes as inserting needle for biomedical sensing [2-6], vertical active devices like diodes and transistors [7]-[9], microwire force sensor arrays with embedded p-n diodes for both force and temperature detection [10], silicon microwire arrays for photovoltaics and solar fuel generation [11] etc. There are various ways of fabricating Si microneedles such as chemical vapor deposition (CVD), molecular beam epitaxy (MBE), laser ablation, etching techniques, vapor-liquid-solid (VLS) process etc. Among them vapor-liquid-solid process [12] is the most prominent method for Si microneedle sysnthesis.

Silicon microneedles are being extensively experimented for applications as sensors, high-efficiency photovoltaic solar cells etc. nowadays and their importance in such applications has motivated this thesis work. Proper mathematical modeling and characterization of the physical and electrical properties of Silicon microneedles are required for their successful utilization and growth. Literature shows that most previous researchers reported intrinsic type Si microneedles grown by VLS using only Si gas source. The main goal of this research work is the modeling and detail analysis of physical and electrical properties of phosphorus doped Silicon microneedle grown by Vapor-Liquid-Solid (VLS) mechanism.

1.2 State of the problem

Intrinsic type Si micro needles grown by VLS method using only Si gas source has been reported by several researchers previously [1]-[3], [5]-[6], [8] but these are not suitable for many applications due to its high resistivity (~ 10^4 Ω-cm). High resistivity of intrinsic Si microneedles is a barrier for collecting small valued neural signals and undoped Si microneedles cannot be used for device fabrication. Therefore, doping of Si needles to

produce highly conductive needles is demanded. Conventional thermal doping uses very high temperature (around 1100°C) by which satisfactory doping can be achieved but the high temperature may be detrimental to the on-chip devices [8]. On the other hand, low temperature (around 900°C) diffusion cannot dope the needle fully; it was observed that at 900°C the depth of the doping was 0.5µm from surface of the needle sidewall [9].Thus conventional thermal doping is not a practical approach of realizing highly doped conductive Si-microneedles because of temperature limitations. However, considering these limitations, highly conductive Silicon micro needle can be grown at a low temperature around 700°C by introducing *in-situ* doping into the VLS growth method [12]. Phosphorus-doped n-type microneedles have been grown via *in-situ* doping into VLS mechanism using gold (Au) as the catalyst particle with disilane (Si_2H_6) as Si source and phosphine (PH_3) as dopant source [13].

It is evident from the experimental data [37] that phosphine flow changes the growth kinetics and electrical properties of the microneedles. Experimental observation reveals that phosphorus doping changes the growth characteristics of the microneedles significantly compared to the intrinsic one. The growth rate decreases with the increment of phosphorus doping. This research work has explained the reason behind the decreasing trend of the growth rate of phosphorus doped Si microneedles along with successful analysis and modeling. Phosphorus incorporation also affects the diameter dependence of the Si microneedles which is discussed in detail in this work. Again phosphorus doping changes the electrical properties of the needles. Since VLS method requires metallic (Au) catalyst, at the end of growth metal-Si alloy remains at the tip of the miconeedles. So, a metal-Si junction is expected. The experimental result shows linear I-V characteristics. A complete analysis and model of the electrical behavior of phosphorus doped Si microneedles is also presented in this work.

1.3 Objectives

The thesis concentrates on the analytical modeling of the physical properties like the growth rate and diameter of the microneedle depending on selected growth conditions i.e. doping level and Au dot diameter. It also includes detailed analysis of the electrical properties of n-Si microneedle. The work consists of derivation of analytical expressions

and numerical simulations. This thesis work has the following objectives related to phosphorus doped silicon microneedle grown by *in situ* VLS method:

i. To model the growth rate of phosphorus doped silicon micro needle as a function of Au dot size and doping level.
ii. Modeling of the diameter of the needle as a function of the Au dot size and doping level.
iii. Analytical modeling of the current-voltage (I-V) characteristics of phosphorus doped silicon microneedle.

The results of this work can be applied to predict the length, diameter and electrical properties of the needle required for certain applications.

1.4 Approach

The growth rate of phosphorus doped silicon microneedle is influenced by several factors like the properties of the liquid alloy, the rate of gas flow, Au dot size, doping level, the ambient temperature and pressure etc [13]. At the very first, the effect of changing doping level on the growth rate will be analyzed. According to previous reports phosphorus doping results in a decrease in the growth rate [17]. A mathematical model representing the relationship between the growth rates and doping level will be developed considering active surface blocking caused by phosphorus [17], gas phase reaction of disilane (Si_2H_6) and phosphine (PH_3). Similarly for a constant doping level the growth rate variation of phosphorus doped Si microneedles will be investigated as a function of Au dot size. Due to the change of Au-dot size, the liquid-gas interface area and the curvature of the droplet changes. As per Gibbs-Thomson effect, the change in curvature of the interfacial area causes change in chemical potential between the vapor and liquid phase. Therefore, the absorption tendency of Silicon and phosphorus atoms from gas phase to liquid phase is altered and hence the growth rate of microneedles changes. Again diffusion of the silicon atoms towards the tip of the needle contributes to the growth rate. All these factors will also be incorporated in growth rate modeling.

The diameter of the needle depends on the Au-Si liquid alloy droplet size, which is directly related to the Au-dot size. However, the size of the droplet is affected by the surface tension

of liquid Au-Si alloy droplet as well as the wetting of Si by liquid Au-Si alloy [18]-[21]. All these factors will be considered for the modeling of the needle diameter as a function of Au dot size. Similarly the effect of doping on the diameter will be analyzed.

Since VLS method requires metallic (Au) catalyst, at the end of growth metal-Si alloy remains at the tip of the miconeedles. So, a metal-Si junction is expected. Related physics of metal-semiconductor junction, Ohmic contact, Fermi level, Schottky Barrier and band theory [22], electron transport process [23],[24] will be used to analyze the I-V characteristics.

All the results of this work will be compared to experimental data to justify the compatibility of the models.

1.5 Organization of the thesis

This thesis work consists of six chapters:

Chapter 1 is concentrated on the introductory discussions on Si microneedle, purpose and scope of the work, background and present state of the problem, objective and methodology.

In chapter 2, review of previous work, a brief overview of the different methods of microneedles fabrication, application of Si microneedle, the VLS mechanism and the experimental procedure of microneedle growth process is covered.

In chapter 3, the growth rate dependency of phosphorus doped Si microneedle on the doping level and Au dot diameter is analyzed. Mathematical models of the growth rate for both growth conditions are developed and the models are compared with the experimental data in each case.

Chapter 4 includes the modeling of needle diameter as a function of Au-dot size. At the same time the effect of doping on the diameter has been analyzed in this chapter. Detailed analysis and explanation of the diameter dependency is presented and mathematical models are derived to compare with the simulation data.

In chapter 5, the electrical properties of phosphorus doped Si microneedle are analyzed and the experimental I-V characteristics data are compared with the simulation results.

Chapter 6 is the concluding chapter. It contains the summery and outcome of the thesis work. Finally some proposals for future works are highlighted. All references are placed at the end of this thesis.

CHAPTER 2

MICRONEEDLE FABRICATION

2.1 Introduction

MEMs is an emerging technology which uses the tools and techniques that were developed for the integrated circuit Industry to build microscopic machines. It merges at the nano-scale into nano-electromechanical systems (NEMs) and nanotechnology. MEMs are separate and distinct from the hypothetical vision of molecular nanotechnology or molecular electronics. MEMs are made up of components between 1 to 100 micrometers in size (i.e. 0.001 to 0.1 mm), and MEMs devices generally range in size from 20 micrometers (20 millionths of a meter) to a millimeter (i.e. 0.02 to 1.0 mm). The real power of this technology is that many machines can be built at the same time across the surface of the wafer, with no assembly required. Since it is a photographic-like process, it is just as easy to build a million machines on the wafer as it would be to build just one. MEMs technology can be implemented by different materials and manufacturing techniques. The basic techniques include patterning, wet etching, dry etching, electro discharge machining (EDM), chemical vapor deposition (CVD), vapor liquid solid (VLS) and others. There are four components of MEMs and they are: microsensors, microelectronics, microactuators and microstructures.

Sensors gather information from the environment through measuring mechanical, thermal, biological, chemical, optical, and magnetic phenomena. The electronics then process the information derived from the sensors and through some decision making capability direct the actuators to respond by moving, positioning, regulating, pumping, and filtering, thereby controlling the environment for some desired outcome or purpose. The microstructure of a material can strongly influence physical properties such as strength, toughness, ductility, hardness, corrosion resistance, high or low temperature behavior, wear resistance, and so on, which in turn govern the application of these materials in industrial practice. Microneedles are microstructures of special shape with are compatible for Si IC technology.

In this chapter, we will review the previous work regarding microneedle fabrication in section 2.2. Section 2.3 presents some prominent fabrication process for Si micro and nanowire fabrication and section 2.4 will present some applications of Si microneedles. The vapor liquid solid mechanism will be discussed in section 2.5 and section 2.6 will give an overview of the experimental procedure of fabrication of n-Si microneedle.

2.2 Review of previous work

The Vapor Liquid Solid (VLS) mechanism, first proposed by Wagner and Ellis [12] in the mid-1960s, is the key mechanism for silicon-wire growth. Their proposed VLS mechanism is based on two observations: that the addition of certain metal impurities is an essential prerequisite for growth of silicon wires in experiments, and that small globules of the impurity are located at the tip of the wire during growth. From this, Wagner and Ellis deduced that the globule at the wire tip must be involved in the growth of the silicon wires by acting ‘‘as a preferred sink for the arriving Si atoms or, perhaps more likely, as a catalyst for the chemical process involved’’ [12]. The vapor liquid solid process is a mechanism of forming needle-like crystal directly. In this method dots of metallic catalyst (generally Au-dots) are formed on Si substrate. Then the substrate with Au-dots is heated in a vacuum chamber to temperatures above about 363°C and small liquid Au–Si alloy droplets will form on the substrate surface.

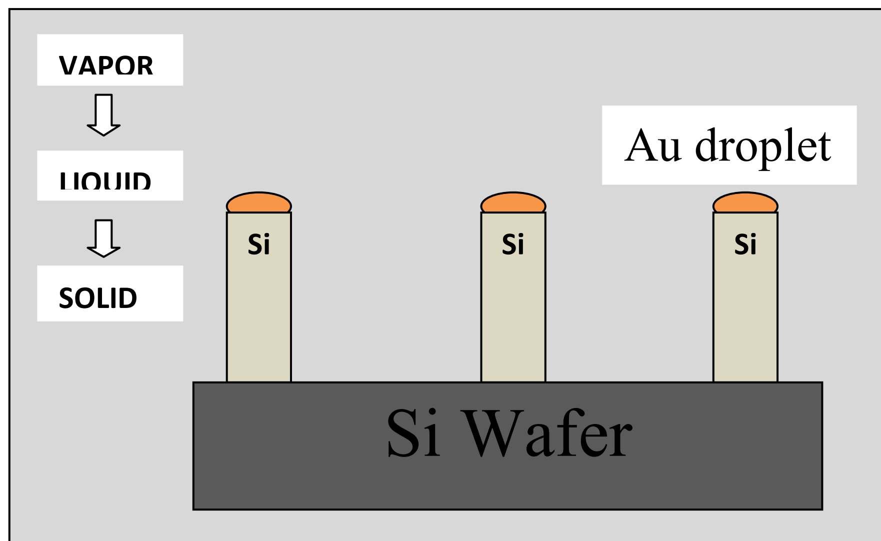

Fig.2.1: Si microneedle grown on Si substrate by VLS method

Exposing such a substrate to a gaseous silicon precursor, precursor molecules will crack on the surface of the Au–Si alloy droplets, whereupon Si is absorbed into the droplet. The silicon supply from the gas phase causes the droplet to become supersaturated with Si until silicon freezes out at the silicon/droplet interface. Thus Si atoms precipitate at the interface at the alloy droplet and substrate. The continuation of this process then leads to the growth of a wire with the alloy droplet riding atop the growing wire as shown in Fig.2.1.

However, since 1964 researchers are using this method as an effective way of fabricating needle like structures both in micro and nano scale for various applications [1]-[6]. But most previous researchers reported about intrinsic type microneedle and the major drawback of these intrinsic type needles is high resistivity which is an obstacle towards collecting small signals. A group of researchers, M.S. Islam *et al* in the Toyohashi University of Technology; Japan introduced an alternate approach by incorporating *in situ* doping into VLS growth system and thus they obtained doped Si microprobes at low temperature (around 700°C) [13],[15],[16]. This method of *in situ* doping solved the temperature and resistivity problems to a great extent. Both p-type and n-type microneedles were grown successfully by the group. Experimental data was collected and reported where some deviation in growth kinetics and electrical characteristics was found in case of phosphorus doped n-Si microneedles.

2.3 Fabrication process

There are many bottom-up and top-down fabrication process of silicon wires. A short summery of the different fabrication methods are given below [25]:

2.3.1. Chemical Vapor Deposition (CVD)

CVD derives its name from the way the silicon, required for wire growth, is provided. In CVD, a volatile gaseous silicon precursor, such as silane, SiH_4, or silicon tetrachloride, $SiCl_4$, serves as the silicon source. It is transported to the deposition surface at which the precursor reacts, and is cracked into its constituents as depicted in Fig.2.2a. Originally, CVD was devised for the deposition of high-purity films. Contaminations such as gold particles, however, were found to cause anisotropic growth of silicon, that is, the growth of silicon wires. CVD allows epitaxial growth of silicon wires, with the growth velocity

varying from about 10^{-2} to 10^{-3} nm/min, depending on temperature and type of Si precursor used. Furthermore, CVD offers broad possibility of modifying the properties of the silicon wires in a controlled fashion. A variety of derivatives of CVD methods exist. These can be classified by parameters such as the base and operation pressure or the treatment of the precursor. Since silicon is known to oxidize easily if exposed to oxygen at elevated temperatures, it is crucial to reduce the oxygen background pressure in order to be able to epitaxially grow uniform silicon nanowires.

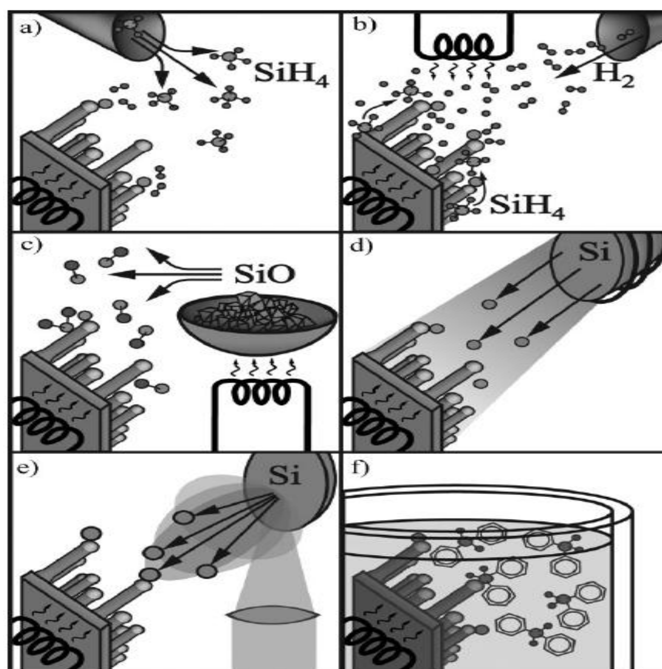

Fig.2.2: Schematics of experimental setups for silicon wire growth.
a) CVD, b) annealing in reactive atmosphere, c) evaporation of SiO,
d) MBE, e) laser ablation, and f) solution-based growth [25].

In particular, when oxygen-sensitive catalyst materials are used, it turns out to be useful to combine catalyst deposition and wire growth in one system, so that growth experiments can be performed without breaking the vacuum in between. In any case, it is useful to lower the base pressure of the CVD reactor down to high or even ultrahigh vacuum, which reduces unwanted contamination and enables growth at lowered temperatures. The pressures during growth depend mainly upon the gaseous silicon precursor and its cracking probability at the catalyst surface. By modifying the precursor before reacting with the sample surface, the temperature budget of the substrate can be lowered. In cases where the thermal load is

critical or where a high supersaturation of the droplet is necessary, wire growth can be enhanced using plasma-enhanced CVD (PECVD).

2.3.2 Annealing in Reactive Atmosphere

Already pioneered in the early 1960s, a method to synthesize silicon whiskers was to expose a crystalline silicon, contaminated with certain metal impurities to reactive gases like hydrogen, iodine, or bromine, and heat it up to about 900°C. At such temperatures, the gases can react with the solid silicon, locally generating silicon compounds like SiH_4, SiI_2, or $SiBr_2$. The metal-droplet contamination acts as catalyst and growth proceeds as in conventional CVD. The main advantage of this method is clearly its technical simplicity, which is presumably the reason why it was used in the early works on silicon-wire growth. In some sense, this method can be seen as the predecessor of wire growth by conventional CVD. As schematically indicated in Fig.2.2b, a modification of this method, used nowadays, is hot-filament CVD. The schematic is shown in Fig.2.2b.

2.3.3 Evaporation of SiO

A cost-effective method to produce silicon nanowires on a large scale is to evaporate solid silicon monoxide, SiO (Fig.2.2c). A two-zone tube furnace connected to an inert gas supply and small amounts of SiO granulate are the basic requirements for the synthesis of silicon nanowires. Crucial for growth is a temperature gradient from about 1350 to 900°C along the tube of the furnace. SiO is evaporated at the hotter end of the tube, flows with the gas stream to the cooler part, where it undergoes a disproportionation reaction into Si and SiO_2, thereby forming the nanowires. In principle, two different growth methods are possible: growth with and without metal catalyst. Growth assisted by the presence of a metal catalyst is relatively rapid. Consistent with the concept of VLS growth, the diameters are determined by the size of the catalyst particle, although the interplay between the nanowire and the catalyst droplet seems to be more complex compared to normal CVD growth. As a consequence of the disproportionation reaction, the diameter ratio between crystalline core and amorphous shell remains approximately constant. The second growth mode, metal-catalyst-free growth, has been originally proposed for growth via laser ablation, where it

was observed that nanowires can be catalyzed by silicon dioxide. Remarkable about this oxide-assisted growth (OAG) is that SiO_2-containing targets clearly raise the yield of the final amount of silicon nanowires compared to pure silicon targets or mixed silicon–metal targets.

2.3.4. Molecular Beam Epitaxy (MBE)

In MBE, a solid high-purity silicon source is heated until Si starts to evaporate. Fig.2.2d schematically depicts an MBE setup. A directional gaseous beam of silicon atoms is aimed at the substrate, on which the atoms adsorb and crystallize. To reduce contamination, the base pressure of an MBE system is usually kept at ultrahigh vacuum, allowing monitoring the growth using reflection high-energy electron diffraction or other surface sensitive examination methods. Similar to CVD, MBE was initially designed for epitaxial layer-by-layer deposition only.

Yet, metal contamination was also found to cause silicon-wire growth in this case. Differing from CVD, no precursor gas is cracked at the surface of the liquid metal–silicon alloy. Therefore, the latter cannot be treated as a classical catalyst anymore. In MBE, two silicon fluxes govern wire growth. First, the direct flux of silicon from the silicon source; and second, the flux of diffusing silicon adatoms from the silicon substrate surface. The nanowires produced by MBE—usually grown on Si(111) substrates—are epitaxial and <111> oriented. MBE offers excellent controllability in terms of the incoming flux, such that doped wires or heterostructures can be grown by switching between evaporation sources. One disadvantage of MBE, however, is that the method is limited with respect to the minimally possible Si-nanowire diameter. Only wires with diameters greater than about 40nm can be obtained, which seems to be a consequence of the Gibbs–Thomson effect, and the fact that only small Si supersaturations are achievable by MBE. Another disadvantage of MBE is the low nanowire growth velocity of a just a few nanometers per minute.

2.3.5. Laser Ablation

The silicon nanowires produced by laser ablation differ in many aspects from the MBE grown whiskers. One can easily obtain large quantities of ultrathin nanowires with high aspect ratio. As schematically displayed in Fig.2.2e, a high-power pulsed laser ablates

material from a mixed Si–catalyst target, which is placed in a tube furnace held at high temperatures and purged with an inert gas. The silicon material ablated from the target cools by colliding with inert-gas molecules, and the atoms condense to liquid droplets with the same composition as the target. Thus, these nanoparticles contain both Si and the catalyst material. According to the VLS mechanism, silicon nanowires start to grow once the catalyst gets supersaturated with silicon and proceeds as long as the catalyst nanoparticles remain liquid. The advantages of laser-ablated nanowire production are manifold. First, there is no need for a substrate. Second, the composition of the resulting nanowires can be varied by changing the composition of the laser target. By adding, for example, SiO_2 to the target, single-crystalline silicon nanowires with varied amorphous SiO_x shell thicknesses can be obtained in a single processing step, with silicon-core diameters as low as 5nm and varying shell thicknesses of about 10 nm. Due to the high growth temperatures, catalyst metals such as Fe, possessing a high eutectic temperature, can be used. The resulting nanowire growth velocities are typically of the order of micrometers per minute.

2.3.6. Solution-Based Techniques

Wire growth can not only take place in gaseous environments, but also in liquid media. These solution-based growth techniques are the methods of choice for high-yield silicon-nanowire production. One method utilizes highly pressurized supercritical organic fluids enriched with a liquid silicon precursor, such as diphenylsilane, and metal catalyst particles, as indicated in Fig.2.2f. At reaction temperatures above the metal–silicon eutectic, the silicon precursor decomposes and silicon forms an alloy with gold. Analogously to the VLS mechanism, the alloy droplet in this supercritical–fluid–liquid–solid (SFLS) method starts to precipitate a silicon nanowire once the alloy gets supersaturated with silicon. Crystalline nanowires with diameters as low as 5nm and several micrometers in length have been fabricated using this approach. Similar to the VSS mechanism, silicon-nanowire growth via a solid catalyst particle has also been demonstrated for the solution-based method. Micrometer-long nanowires were synthesized at a temperature of merely 500^oC using copper particles as catalysts. Another high-yield silicon-nanowire production method is the so-called solution–liquid–solid (SLS) method. Here, the growth environment is not a

supercritical liquid, but an organic solvent at atmospheric pressure, and the production of micrometer-long crystalline wires, 25nm in diameter, has been demonstrated. The SLS method probably represents the most-cost-effective nanowire-production method, as it can be realized without high-priced equipment.

2.3.7. Top-down Fabrication Methods

In addition to the different bottom-up fabrication methods discussed above, several attractive top-down approaches for the fabrication of single crystalline silicon nanowires exist. Due to the processing-related differences, one should distinguish between the fabrication of horizontal nanowires, that is, nanowires lying in the substrate plane, on the one hand, and the fabrication of vertical nanowires, that is, nanowires oriented more or less perpendicular to the substrate, on the other. Horizontal silicon nanowires are mostly fabricated from either silicon-on-insulator (SOI) wafers or bulk silicon wafers using a sequence of lithography and etching steps, often employing electron-beam lithography and reactive ion etching. In most cases, horizontal nanowire processing is finalized by an oxidation step, which also serves to reduce the silicon nanowire diameter. In this way, diameters well below 10nm have been achieved in the past. No further thinning of the nanowires is necessary in the so-called superlattice nanowire pattern-transfer (SNAP) technique. In this approach a differentially etched GaAs/AlGaAs superlattice is used as a stamp to transfer thin metal lines onto the substrate, which can then be used for further processing. Using standard silicon technology, vertical silicon nanowires can also be produced. Often, reactive-ion etching is used to etch vertical silicon nanowires out of a silicon wafer. The diameter of the nanowires is defined by a lithography step preceded by reactive ion etching. A variety of different nanostructuring methods, such as electron-beam lithography, nanosphere lithography, nanoimprint lithography, or block-copolymers have been employed for this purpose. As an alternative to reactive-ion etching, the so-called metal-assisted etching of silicon attracted some attention recently. In this approach Si is wet-chemically etched, with the Si dissolution reaction being catalyzed by the presence of a noble metal that is added as a salt to the etching solution. Alternatively, also a continuous but perforated noble-metal film can be used. During etching, this perforated metal film will etch down into the silicon producing vertical silicon nanowires at the locations of the holes in the metal film.

2.4 Applications of microneedles

Needle like microstructures has a huge prospect as MEMs. MEMs has several applications in the fields of biotechnology, medicine, sensors etc. and microneedles fabricated using MEMS technology are being used as biomedical sensors due to their special needle like shape and mechanical strength [10]. Silicon nanowires are also being explored by researchers as they are another major candidate for sensor applications but they lack the mechanical strength offered by Si microneedles. Mechanically robust structures are required during penetration into tissues such as brain, peripheral nerves etc. Microstructures are mechanically strong and hence suitable for certain sensor applications. There are also many other potential applications demonstrated by Silicon microwires. Here are a few applications of microneedles:

2.4.1 Force and temperature sensors

Recently A. Ikedo *et al* have proposed an out-of-plane high-aspect-ratio microneedle array sensors for use in multisite contact force and temperature detection with high spatial resolution using the piezoresistance effect of semiconducting materials [10].

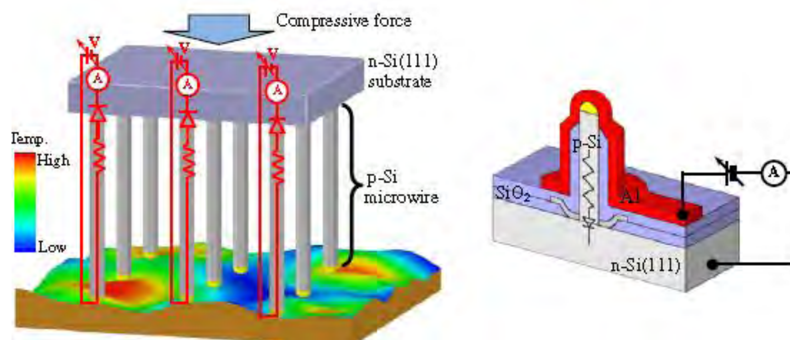

Fig.2.3: Out-of-plane silicon microwire-based artificial whisker array sensor by selective VLS growth of p-silicon on n-silicon [10]

Both force- and temperature-sensitive microwire sensor arrays have potential in numerous applications, including artificial electronic fingertips in a robot hand/prosthetics, multisite sensing of contact force, shear force, surface roughness and slip, and local temperature sensing capabilities. The following figure illustrates the force and temperature sensor:

2.4.2 Biotechnology

The electrical recording of the cell response in living cultures to an external stimulus is a fundamental method for drug development and disease studies. Various MEMs are used for DNA amplification and identification, biochips for detection of hazardous chemical and biological agents, and for high throughput drug screening and selection. J. Held *et al* [6] have reported the use of microneedle for electroporation of adherently growing cells and intracellular recording with focus on the influence on external factors on the cell behavior. The following figure shows how the microneedles are used for intracellular recording:

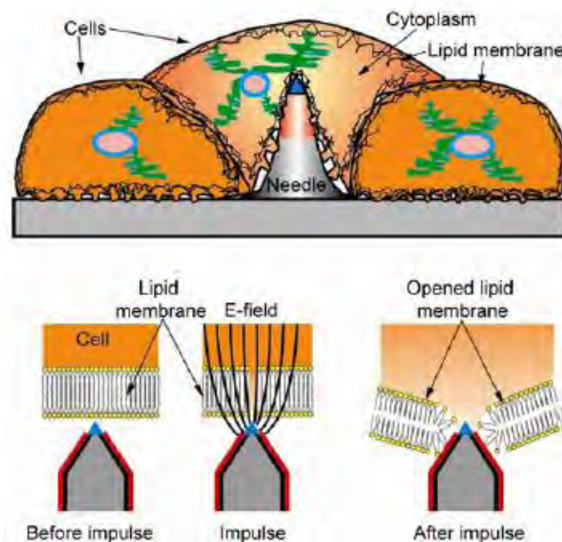

Fig.2.4: Microneedle electrode grown by dry etching inserted into cells for intracellular recording [6]

2.4.3 Medical Science

There are numerous applications for MEMs in medical science. Pressure sensors for blood pressure and respiration monitoring system, barometric pressure sensing, in kidney dialysis monitoring system, drug delivery etc. are some successful applications of MEMs in medicine. MEMs electrodes are now being used in neuro-signal detection and neuro-stimulator applications. T. Kawano *et al* have reported the development of neural recording chip device with penetrating Si microprobe electrode array using IC-process [3]. These microneedles have prospective applications in the chemical and biomedical fields for

localized chemical and programmable drug delivery system [7],[14]. Following figure illustrates hollow out-of-plane microneedle fabricated for drug delivery:

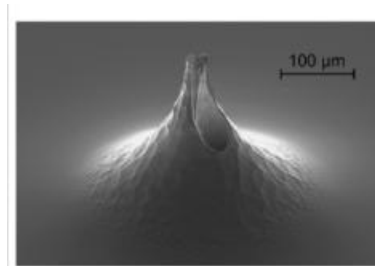

Fig.2.5: A pointed single crystal silicon needle [14]

2.4.4 On-chip devices

K. Takei *et al* have reported the fabrication of Si microprobes and on-chip NMOSFETS and also tested the electrical characteristics as well as mechanical characteristics of the needles so that they can be used to collect neural signals from human brain [4]. T. Kawano *et al* have reported micro-Si Probe Electrode Arrays With On-Chip MOSFETs on Si (111) Substrates using selective vapor-solid-liquid method [9] (Fig.2.6).

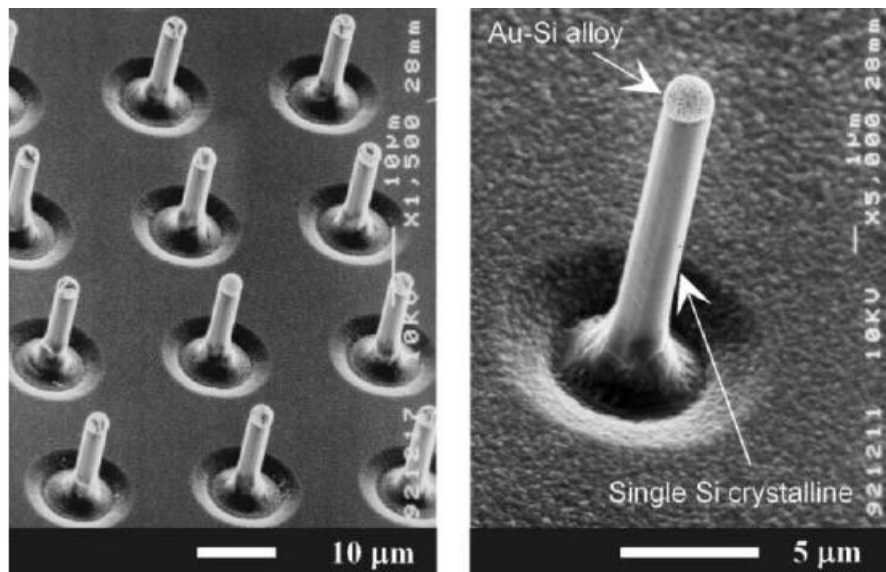

Fig.2.6: SEM views of Si probes grown by selective VLS growth using a Au catalyst and SiH gas. The VLS growth realizes micro-Si probes with a Au–Si alloy dot at the tip and a single crystalline Si body [9]

Realization of Si vertical surround gate FET (Fig.2.7) is reported by V. Schmidt *et al* [7]. This kind of vertical surround gate can also be fabricated in micro scale which will be suitable for use as sensors.

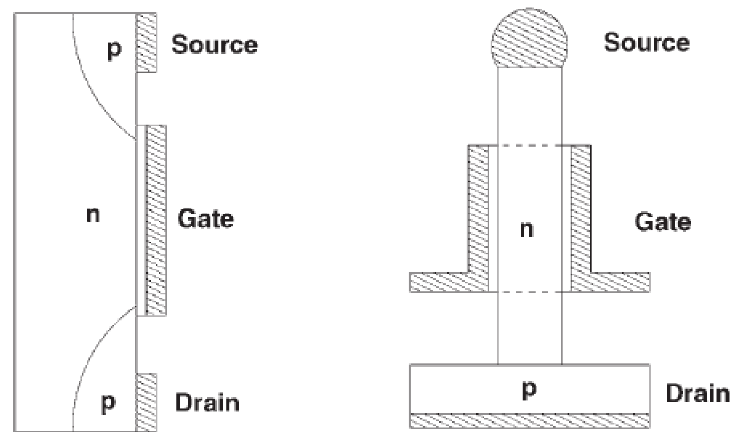

Fig.2.7: Schematics of conventional p-channel MOSFET and a silicon nanowire vertical surround-gate field-effect-transistor grown by VLS method [7].

2.4.5 Photovoltaics

Silicon microwire arrays have recently demonstrated their potential for low-cost, high-efficiency photovoltaics and photoelectrochemical fuel generation. T. C. Adele *et al* have demonstrated wafer scale epitaxial growth of Si microwire arrays for photovoltaic application [11]. Following figure shows epitaxially grown Si microwire arrays for photovoltaic application:

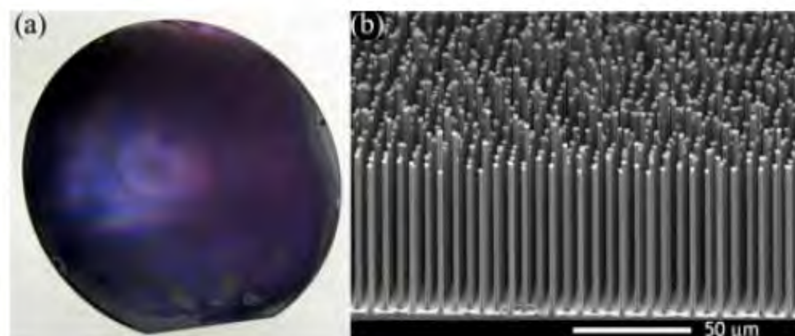

Fig.2.8: Photograph of a six-inch wafer covered in Si microwires (left) and SEM image of these wires (right) [11]

2.5 Vapor-liquid-solid mechanism

2.5.1 Introduction

Vapor Liquid Solid mechanism was first introduced by Wagner and Ellis in 1964 [12] which is a mechanism for the growth of needle like micro and nanostructures. Similar structures can also be grown from Chemical Vapor Deposition (CVD). In CVD method crystal growth is through direct adsorption of Si particles from gas phase onto a solid surface and thus the growth rate is very slow. In VLS mechanism the catalytic liquid alloy works like a tarp and therefore can absorb the atoms from the gas phase rapidly. Thus the growth rate of Si microneedles in VLS method is faster than those grown by CVD and other methods. The VLS mechanism can be described in three stages as shown in the following schematic diagram:

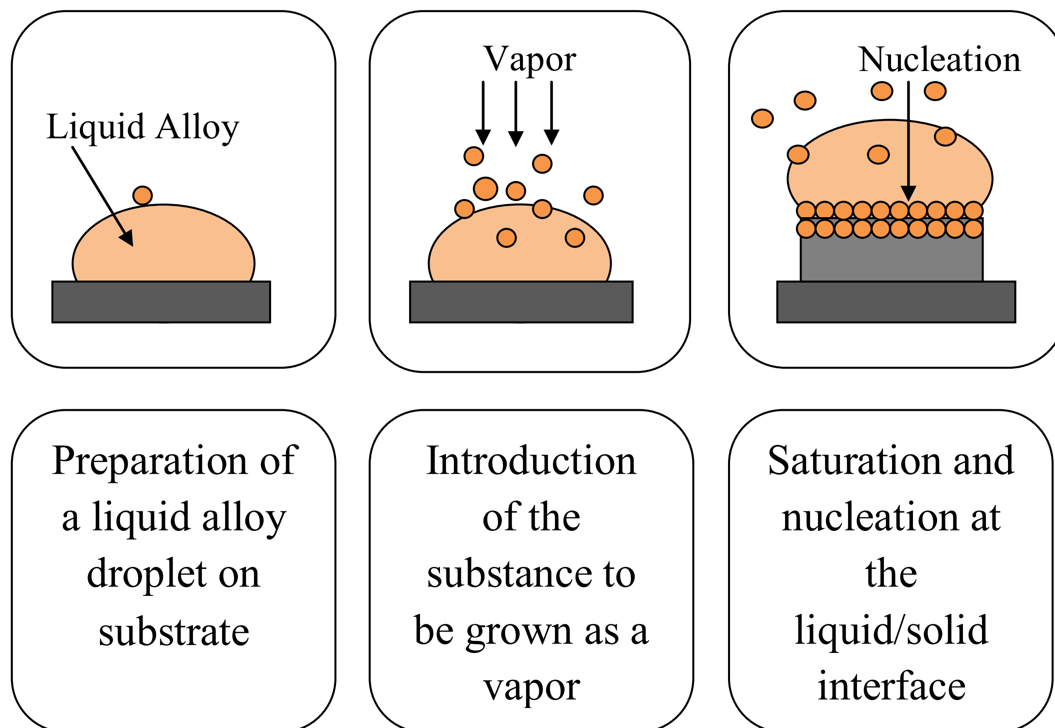

Fig.2.9: Three basic stages of VLS mechanism

2.5.2 Fundamentals of VLS mechanism

Wagner summarized the experimental details, results and VLS theory in a truly elegant way which was further elaborated by Givargizov who developed the experimental observations,

models and theories regarding the VLS process. Wagner summarized the requirements of VLS growth as follows:

- The catalyst or impurity must form a liquid solution with crystalline material to be grown at the deposition temperature.
- The distribution coefficient of the catalyst or impurity must be less than unity at the deposition temperature.
- The equilibrium vapor pressure of the catalyst or impurity over the liquid droplet must be very small. Although the evaporation of the catalyst does not change the composition of the standard liquid composition, it changes the total volume of the liquid droplet. Unless more catalyst is supplied, the volume of the liquid droplet reduces.
- The catalyst or impurity must be inert chemically. It must not react with the chemical species such as by-products present in the gas chamber. The catalyst should not form an oxide, which would impede VLS wire growth.
- The interfacial energy plays a vital role. The wetting characteristic influences the diameter of the VLS grown microneedles. For a given volume of liquid droplet, a small wetting angle results in a large growth area, leading to a large diameter.
- For a compound growth, one of the constituents can serve as catalyst.
- For controlled unidirectional growth, the liquid-solid surface must be well defined crystallographically. One of the simplest methods is to choose a single crystal substrate with desired crystal orientation.
- The catalyst-Si binary phase diagram should not include solid intermediate phases, which could interfere with VLS growth of Si wires.
- The catalyst-Si eutectic temperature should be compatible with the decomposition temperature of the gaseous Si precursor and it should have low solubility in solid Si.

2.5.3 VLS growth process

The Vapor-Liquid-Solid (VLS) method of nano/microwire growth was originally developed and explored by Wagner and Ellis in the 1960's as a means of growing millimeter-scale single crystal whiskers of silicon. This technique essentially involves three phases to achieve the wire growth. A vapor phase precursor is used to supersaturate a liquid catalyst from which a solid phase single crystal is extruded (Fig.2.10). This technique has been primarily characterized by using Au-Si system where Au is used as the catalyst material and some silicon based gas precursor is used to supersaturate and grow the single crystal silicon.

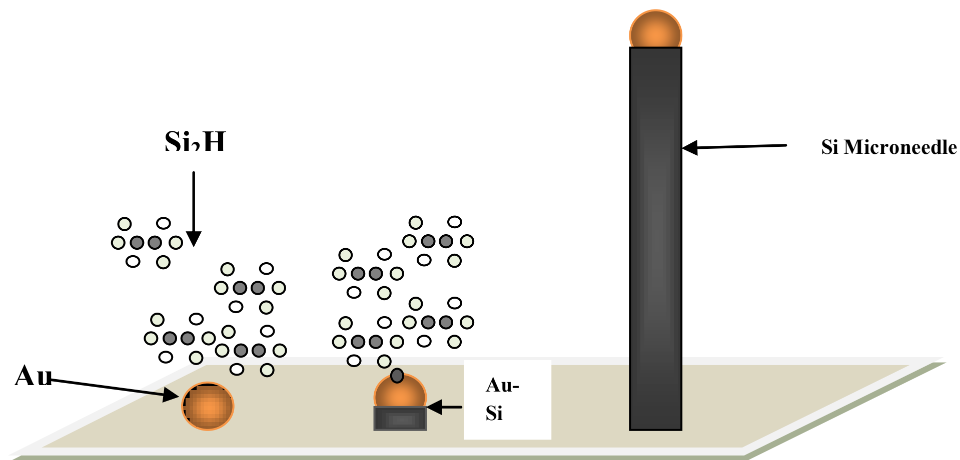

Fig.2.10: Schematic illustration of the VLS process, Si_2H_6 molecules in the vapor phase are flown over metal catalyst particles on a substrate. These molecules decompose preferentially at the catalyst to form a liquid droplet if the sample is held near or above the eutectic temperature. Lastly, a solid single crystal is extruded from the liquid melt

In order to illustrate the process of VLS growth of silicon microneedles, gold (Au) is taken as catalyst material and Si is taken as substrate. There are three steps of silicon microneedle growth and the steps are described in brief as follows:

2.5.3.1 Alloying process

At first a thin layer of gold is deposited on silicon substrate and annealed at an elevated temperature (above the eutectic point of 390°C of the gold-silicon system), which is typically same as growth temperature. During the annealing, silicon and gold react and

form a liquid mixture, which forms a droplet on the silicon substrate surface. During the growth, an equilibrium composition is reached at the growth temperature as determined by the binary phase diagram as shown in Fig.2.11.

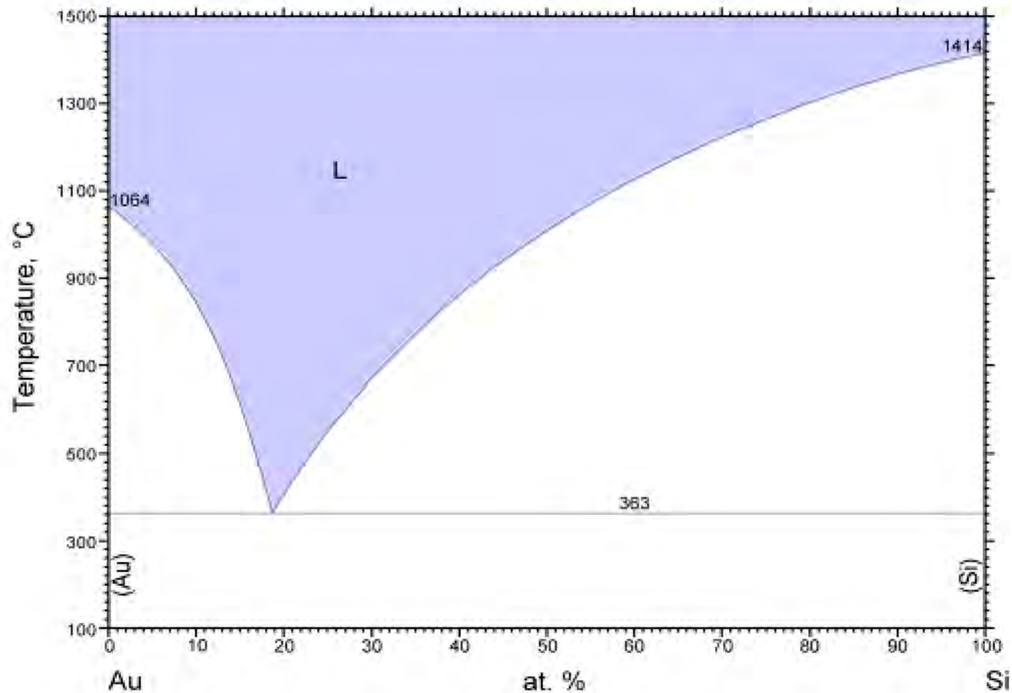

Fig.2.11: Binary Au-Si phase diagram

2.5.3.2 Nucleation process

When Si precursor vapor is introduced from the source the Au-Si droplet acts like a trap and the gas preferentially condenses at the surface of the liquid droplet. Thus the liquid droplet becomes supersaturated with silicon atoms which ultimately diffuse from liquid-vapor interface and precipitate at the solid-liquid interface.

2.5.3.3 Axial growth

Once the Si crystal nucleates at the liquid/solid interface the axial growth starts. Further condensation of Si vapor into the system increases the amount of precipitation. The incoming Si species prefer to condense at the existing solid/liquid interface as this involves less energy requirement. Thus the growth proceeds perpendicularly to the solid-liquid interface and ultimately needles grow as shown in the following figure:

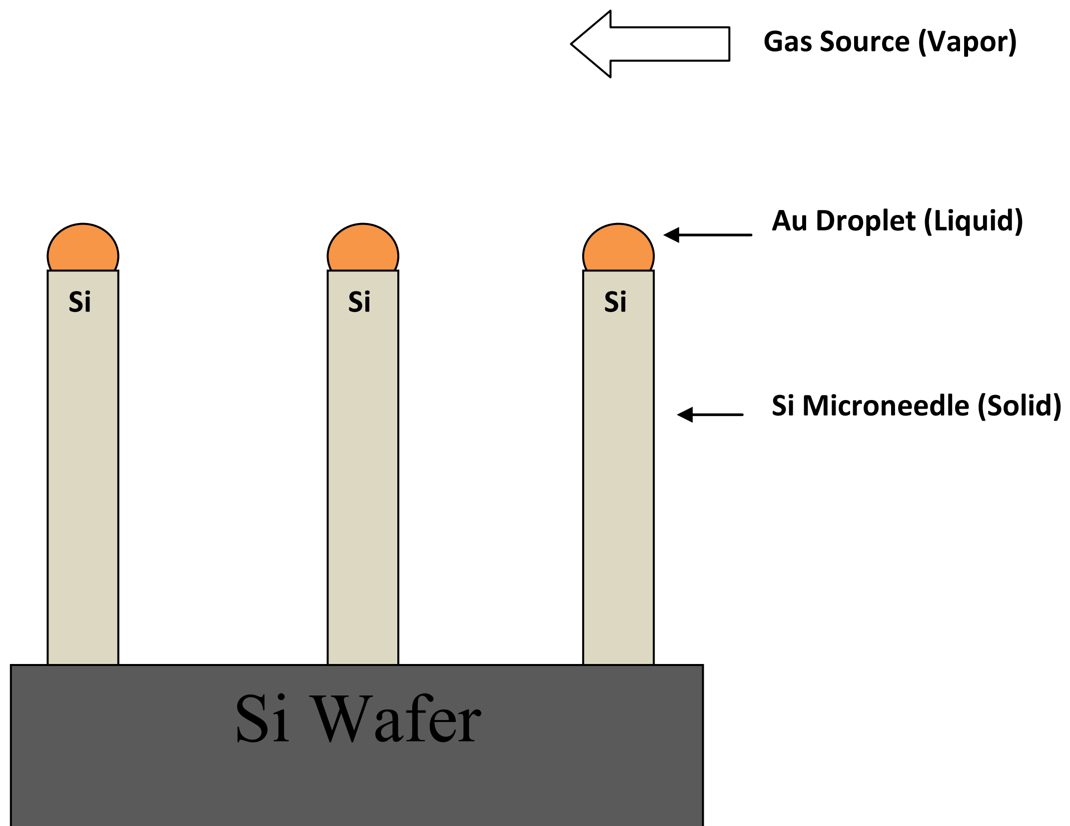

Fig.2.12: Silicon microneedles grown by Vapor-Liquid-Solid mechanism

2.6 *In situ* doped VLS

Incorporating *in situ* doping into VLS growth system doped Si microneedles can be grown at low temperature (around 700°C) [13]. In this method, dopant is introduced as vapor during VLS growth and thus the needles are doped as desired. The doping concentration can be controlled by changing the flow rate of doping species. A group of researchers, at Toyohashi University of Technology, Japan; grew phosphorus doped n-type Si microneedles by incorporating *in situ* doping into VLS growth system at low temperature (~700°C) [13], [15]. The result of the experiment is used in this work for analysis.

2.6.1 n-Si microneedle fabrication

Here n-Si(111) wafer has been used as the substrate in our experiment to grow n-Si microprobes by VLS method. Fig.2.13 illustrates the fabrication process. At first, a layer of SiO_2 with 870 nm in thickness was formed over n-Si (111) substrate as shown in Fig. 2.13a by wet oxidation at 1000ºC. Then the photolithography and etching with buffered hydrofluoric acid (BHF) were carried out to create arrays of circular windows through SiO_2 layer as in Fig. 2.13b.

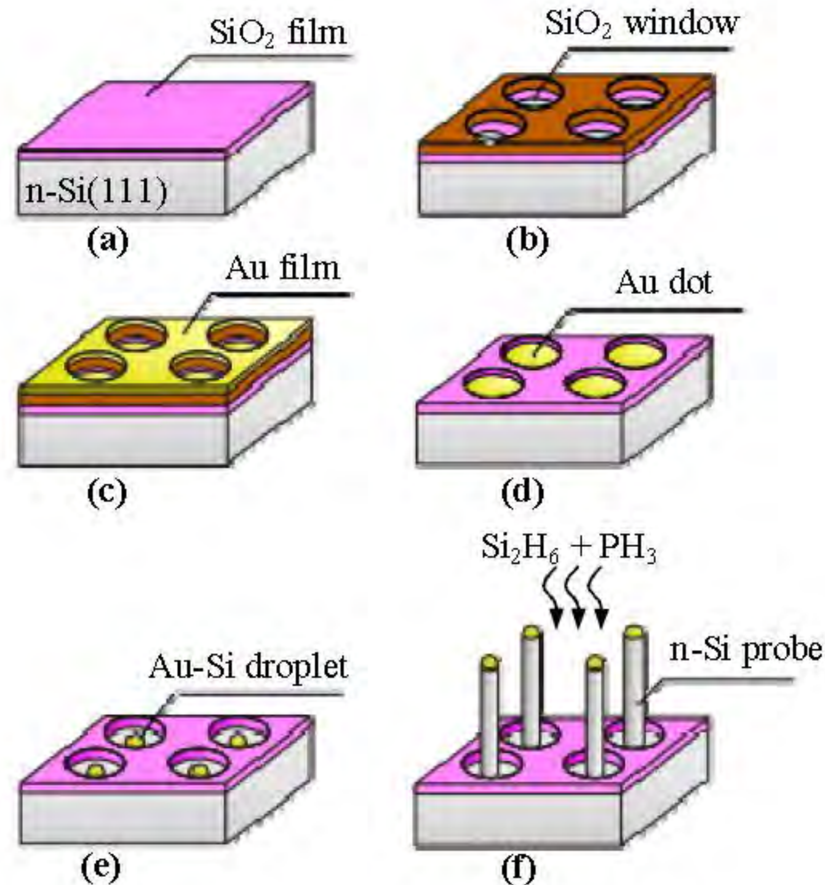

Figure 2.13: Fabrication process of n-Si microprobe array: (a) SiO_2 layer formation; (b) circular window through SiO_2 made by photolithography; (c) Au film deposition; (d) lift-off Au from resist-site; (e) annealing to form Au-Si alloy droplet; (f) introduction of mixed gas of PH_3 and Si_2H_6 into the growth chamber and then n-Si microprobes grow by VLS mechanism [13]

A thin film of Au (Fig. 2.13c) with 170 nm in thickness was deposited over this patterned structure by using evaporation technique. Au film from the resist-surface was removed by using a lift-off process, however circular Au dots remained at pre-determined microprobe sites where the Si surface was revealed through SiO_2 window as shown in Fig. 2.13d. Then the sample, having these circular Au dots, was inserted into a high-vacuum gas-source molecular-beam-epitaxy (GS-MBE) chamber.

The chamber was equipped with 100% Si_2H_6 as Si source and 1% PH_3 (diluted in 99%H_2) to facilitate *in situ* doping of the probes grown by VLS mechanism. The system includes

mass flow meters for controlling the flow rates of PH_3 and Si_2H_6 to vary the dopant -to-silicon ratio in the inlet gas system.

The sample was annealed at a temperature around 700ºC to form Au-Si alloy droplets inside the SiO_2 windows as shown in Fig.2.13e. Then, the mixed gas of PH_3 and Si_2H_6 with desired flow rates was supplied to the growth chamber and hence n-Si microprobes with desired doping were grown on n-Si (111) substrate by VLS mechanism as shown in Fig.2.13f.

2.6.2 Results

n-Si microneedles of different sizes at different doping levels were grown. Fig. 2.14 shows the SEM image of a typical 6×7 array of n-type Si microprobes having the length of 54µm and diameter of 3.6µm, which were grown by *in situ* doping VLS growth at 690°C at the growth pressure of 5.3×10-3 Pa using PH_3 flow at a rate of 1.00sccm with Si_2H_6 flow of 1.70sccm for 90 min.

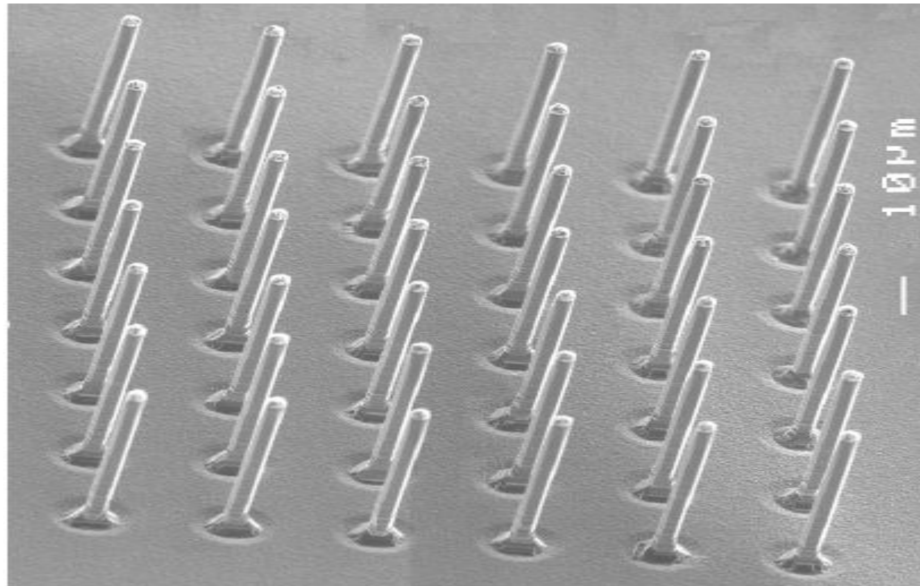

Fig.2.14: SEM image of n-Si microprobe array with probe-length of 54µm and probe-diameter of 3.6µm, which were grown by *in situ* doping VLS with PH_3 = 1.00sccm and Si_2H_6 = 1.70sccm [13]

Diameter and length of the microneedles were measured for various sets of experiments (Table 2.1). The Current- voltage (I-V) characteristic of phosphorus doped n-Si microneedles were also measured by using one contact with tungsten (W) microneedle at

the tip of n-Si microneedle and the other contact was at the base of the microneedle. For the appropriate placing of W-needle at the n-Si microneedle a micromanipulator system was used.

Table 2.1: Experimental data of phosphorus doped n-Si microneedle growth [37]

PH_3 Flow rate (sccm)	SiO_2 Flow rate (sccm)	Temp (C)	Pressure (Pa)	Time (min)	Au Dot Diameter (µm)	Needle Length (µm)	Needle Diameter (µm)
0.15	1.7	690	$5x10^{-3}$	90	4	52.474	2.933
					6	52.10	3.667
					8	47.64	4.467
					10	55	4.8
0.5	1.7	690	$5x10^{-3}$	90	4	53.96	2.267
					6	55.40	3.0
					8	53.92	3.467
					10	56.569	4.267
1.0	1.7	690	$5x10^{-3}$	90	4	51.73	2.267
					6	52.102	3.133
					8	51.73	3.533
					10	55.08	4.467
1.7	1.7	690	$5x10^{-3}$	90	4	62.52	2.533
					6	57.68	2.83
					8	58.44	3.467
					10	-	-

2.7 Conclusion

This chapter briefly presents review of previous work, Si microwire fabrication techniques, VLS growth mechanism, details fabrication steps of *in situ* doped VLS methods used to fabricate n-Si microneedle. At the end, the characterization results obtained from the *in situ* VLS grown n-Si microneedles (using scanning electron microscopy) has been presented.

CHAPTER 3
GROWTH RATE ANALYSIS

3.1 Introduction

At first Wagner and Ellis proposed the model of VLS growth in the 1960's [12]. The fundamental part of the model is that the impurity forms a liquid alloy with low melting point. The gas phase molecules preferably condense on the liquid alloy. Microneedle growth occurs because of the precipitation of the growing material from the impurity. In the case of Si needle growth from Au particles Au-Si forms a eutectic alloy with a melting temperature of 363°C compared to the individual melting temperature of Au and Si is 1063°C and 1412°C respectively. However the model was for intrinsic type Si microneedle and later it was observed by the researchers that doping or impurity affects the growth rate to a great extent.

The growth rate of microneedles by VLS mechanism depends on various factors. Generally the growth rate depends on the size of the droplet, the gas flow rate, temperature, pressure and the characteristics of the doping species in case of *in situ* doped VLS [15]-[18]. However in this research work only the effect of phosphorus doping level and the droplet size on the growth rate is considered individually while considering the other factors constant.

3.2 Effect of phosphorus doping on microneedle growth

Intrinsic type silicon microneedles can be doped by conventional thermal diffusion process at 1100°C after VLS growth of the needles but *in situ* doping VLS can grow doped Si microneedles at lower temperature at around 700°C. Experimental data shows that the incorporation of doping into VLS system changes the properties of the microneedle compared to intrinsic one. The modeling of the growth rate of phosphorus doped silicon microneedle grown at low temperature by Vapor-Liquid-Solid (VLS) mechanism is reported here. The mathematical model of the growth rate of silicon microneedle proposed in this work is supported by the experimental values and a complete theoretical analysis is also included.

3.2.1 Experimental findings

From the experimental data (Table 3.1) it was found that the growth rate of n-Si microneedle decreases with the doping level (PH_3 flow rate) for a fixed Au dot size.

Table 3.1: Growth rate variation of n-Si microneedle from experimental data with various flow of PH_3 at a temperature of 720° C, at a growth pressure of $5X10^{-3}$ Pa and disilane (Si_2H_6) flow rate of 1.7 sccm [37]

PH_3 Flow rate (sccm)	**Growth Rate (nm/min)**
0.04	**700**
0.54	**590**
1.0	**560**

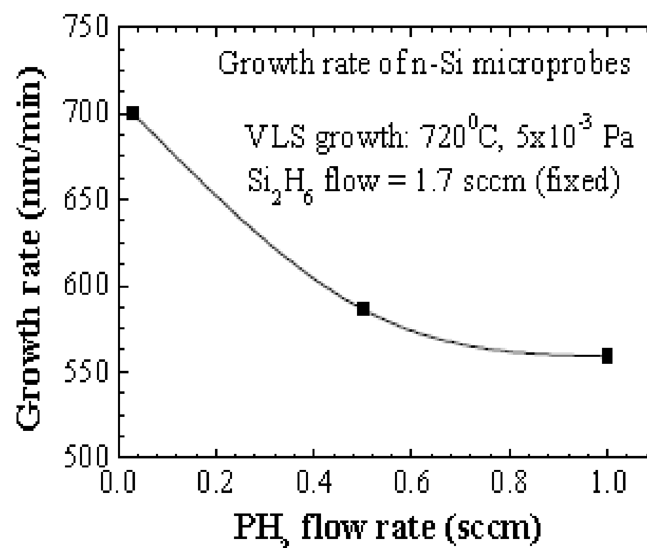

Fig.3.1: Growth rate variation of n-Si microneedle with various flow of PH_3 [13]

3.2.2 Theoretical analysis

Phosphine (PH_3) is added to disilane (Si_2H_6) or Silane (SiH_4) flow frequently for n-type *in-situ* doping during VLS growth of Silicon microneedle or Silicon nano/micowires. The growth rate of undoped Si-nanowire, defined by Givagizov and Chernov[26] is:

$G= k_1(\Delta\mu/kT-k_2/D)^2$ (3.1)

Here k is Boltzmann constant, T(K) is the absolute temperature. k_1(m/s) is the kinetic coefficient of growth of solid-liquid interface between the nanowire tip and the alloy droplet and k_2(m) is a thermodynamic parameter. Both k_1 and k_2 are independent of $\Delta\mu$ and D, but while k_1 is theoretically undetermined k_2 is given by [26]:

$k_2=2\sigma_{SV}\upsilon_o/kT$ (3.2)

Here σ_{SV} (J/m^2) is the appropriately averaged specific surface energy of the solid/vapor interface between the nanowire and the vapors around it, and υ_o (m^3) is the volume of the growth species in the nanowire. D is the diameter of the nanowire. Now it is evident from the above equations that at a fixed temperature, precursor pressure and constant Au-dot diameter the growth rate of nanowire will be constant. This is also true for micron range Silicon wires grown using Vapor-Solid- Liquid method.

It is reported that the introduction of phosphine (PH_3) to the Si-precursor during the Si-microwire and nanowire growth [17], [29] Si-deposition using gas source molecular beam epitaxy [29], phosphorus doping in silicon epitaxy by chemical vapor deposition results in the reduction of Si Growth rate. At low PH_3 flow rate this decrease is linear but as the flow of PH_3 increases the decrease becomes nonlinear. This decrease has been attributed to PH_3 which has almost unity sticking coefficient [33]. The edition of phosphorus does not prevent dopant incorporation, it simply leads to an overall decrease of the kinetics.

3.2.3 Mathematical modeling

Now the model of growth rate as a function of PH_3 flow rate based on the above analysis of the PH_3 can be expressed as:

$G_{Si:P} =G_{Si} -F(J_{PH3})$ (3.3)

Where G_{Si} is silicon growth rate at a particular temperature, pressure and precursor flow rate without P-doping. The constant β is the blocking factor caused by the P-atoms incorporated into the Si-microneedle. The nonlinear decrease of the growth rate has been modeled by $F(J_{PH3})$ where J_{PH3} is the flow rate of phosphine (PH_3). The concentration of the

P atoms incorporated into Si-microneedle can be expressed by the following empirical function [32]:

$$n= A[J_{PH3}]^a \qquad (3.4)$$

Now the poisoning effect caused by the P-atoms must be proportional to the concentration of P-atoms incorporated into the microneedle. Therefore:

$F(J_{PH3})= KA[J_{PH3}]^a$, where K is proportionality constant.

The term KA can be represented as β=KA. Here β is the blocking coefficient attributed to the blocking of available active adsorption sites for Si_2H_6 caused by P-atoms. The final model for growth rate of P-doped Si-microneedle becomes:

$$G_{Si:P} =G_{Si} -\beta[J_{PH3}]^a \qquad (3.5)$$

The parameter 'a' is the adsorption coefficient of phosphorus doping. The coefficients will be different for different experimental setup but once all the parameters such as temperature, pressure, Au-dot size etc. are settled; the coefficients will be constant for the setup. The coefficients can be found for an experimental setup by collecting one set of data experimentally and then by calculating for the proposed model. The experimental setting for this model was as follows:

Growth Temperature= 720°C

Growth Pressure=5x10^{-3} Pa

100% Si_2H_6 Flow rate= 1.7sccm

The Growth rate of Si-microneedle without doping at 720°C can be found from the Arrhenius Plot as follows:

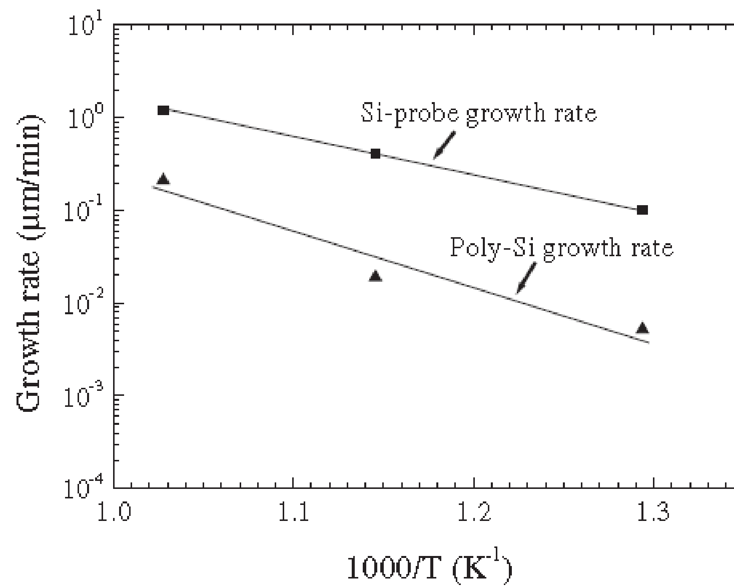

Fig.3.2: Dependence of growth rate of Si probe and that of poly-Si on temperature. Both Si probe and poly-Si [15]

Therefore, G_{Si}= 1.2μm/min=1200nm/min.
The value of the coefficients was found as given below:
β=640 unit and
a=0.08unit
The following Fig.3.2 shows the growth rate variation with doping from the model:

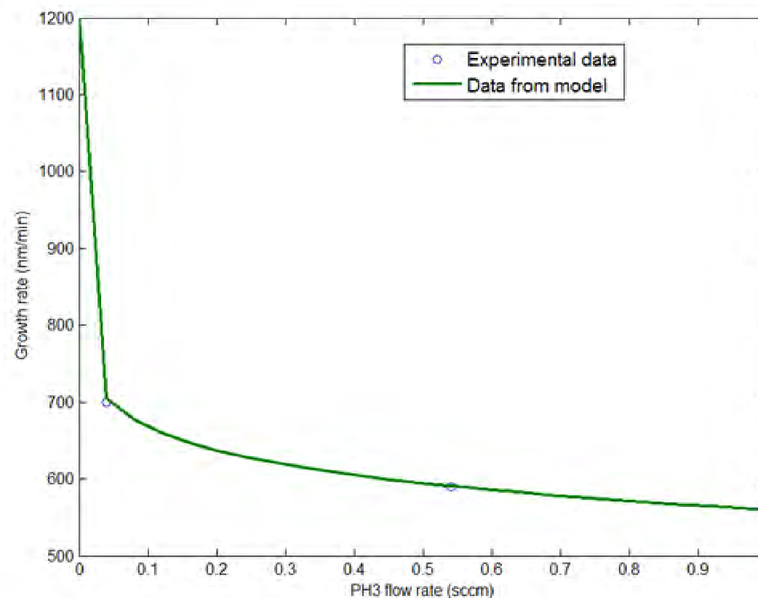

Fig.3.3: Growth rate variation of n-Si microneedle as a function of PH_3 flow rate calculated from proposed model

The following Table 3.2 shows the growth rate variation as a function of flow rate of PH_3 calculated from the proposed model and from experimental values and the agreement was satisfactory.

Table 3.2: Growth rate variation of n-Si microneedle as a function of flow rate of PH_3 calculated from the proposed model and from experimental values

PH_3 Flow Rate (sccm)	Growth Rate (nm/min) Experimental Data	Growth Rate (nm/min) Data from Model
0.04	**700**	**705**
0.54	**590**	**596**
1.0	**560**	**560**

The following Figure (Fig 3.4) shows the growth rate variation as a function of flow rate of PH_3 calculated from the proposed model and from experimental values.

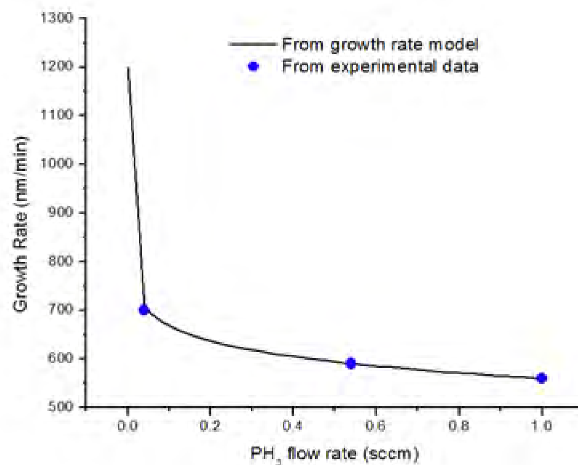

Fig.3.4: Comparison of growth rate variation of n-Si microneedle as a function of doping level from the proposed growth rate model and from experimental data, grown by VLS at a temperature 720°C and at the growth pressure $5x10^{-3}$Pa

From the comparison it is evident that the agreement between the proposed growth rate model and experimental data is satisfactory. For a set of growth conditions the value of the coefficients are constants. Provided that the growth conditions are known, it is possible to predict the growth rate of silicon microneedle for a certain level of phosphine (PH_3) flow rate using the proposed growth rate model.

3.3 The effect of droplet size on microneedle growth

The diameter of the microneedle is directly related to the size of the droplet and it is clear that the larger droplet will result in larger diameter microneedle. The diameter of the microneedle affects the growth rate of the microneedle. Givargizov [26] divided the growth process into three main steps. In the first step, Si precursor molecules are cracked at the surface of the catalyst droplet and Si is incorporated into the droplet. This is called the incorporation step, and the rate (atoms/s) at which it proceeds is called incorporation rate. After incorporation of Si atoms into the catalyst droplet, Si diffuses through the droplet surface towards the needle droplet interface. This is the diffusion step. Finally, Si crystallizes at the liquid-solid interface and forms the Si miconeedle.This is the crystallization step proceeding at a rate (atoms/s) called crystallization rate. Givargizov neglected the diffusion step, arguing that diffusion through a microscopic droplet is simply too fast to seriously affect the growth velocity and ultimately chose crystallization as the rate determining step. According to his observation he reported that comparatively thicker needles grow faster than the thinner needles which could be explained by Gibbs-Thomson effect. However, if the material transports, diffusion of growth material on the substrate and the needle surface is taken into account, then the result would be different [27]. In this work the experimental findings of diameter dependency on growth rate is analyzed in the following sections of this chapter.

3.3.1 Experimental findings

Experimental data of growth-rate of microneedles, having various diameters, was observed carefully (Table 3.3). The diameter of the microneedle grown by VLS mechanism increases with the liquid catalyst droplet size which is controlled by the Au dot diameter. For fixed phosphorus doping level it was observed that the growth rate of microneedles changes with needle diameter and in most of the cases the growth rate of the microneedles decreases with

the microneedle diameter. The plot of growth rate vs. Au dot size for a different set of doping level is shown in Fig.3.5.

Table 3.3: Growth rate for different Au-dot size [37]

PH_3 Flow rate 0.15 (sccm)		**PH_3 Flow rate 0.5 (sccm)**		**PH_3 Flow rate 1.0 (sccm)**		**PH_3 Flow rate 1.7 (sccm)**	
Au Dot Diameter (µm)	**Growth Rate (µm/min)**	**Au Dot Diameter (µm)**	**Growth Rate (µm/min)**	**Au Dot Diameter (µm)**	**Growth Rate (µm/min)**	**Au Dot Diameter (µm)**	**Growth Rate (µm/min)**
4	**0.583**	**4**	**0.5995**	**4**	**0.575**	**4**	**0.695**
6	**0.579**	**6**	**0.616**	**6**	**0.579**	**6**	**0.641**
8	**0.539**	**8**	**0.5991**	**8**	**0.575**	**8**	**0.649**
10	**0.611**	**10**	**0.629**	**10**	**0.612**	**10**	**-**

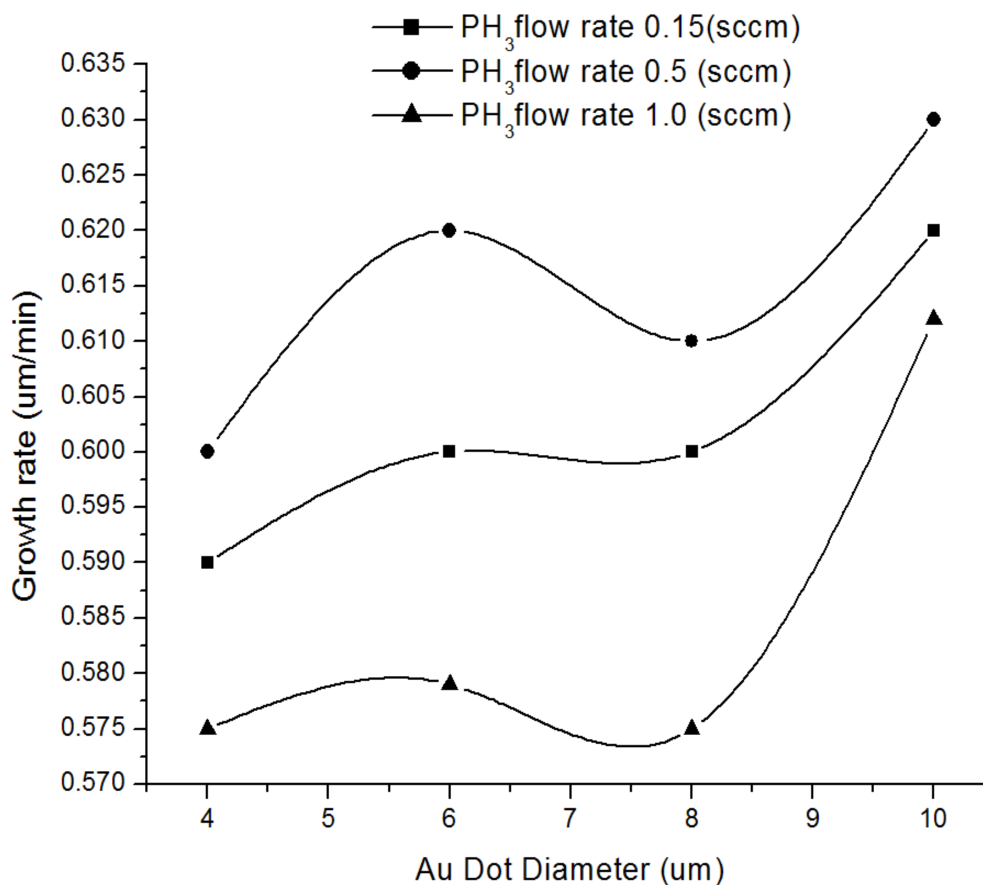

Fig.3.5: Growth rate (µm/min) vs. Au dot size (µm) for various PH_3 flow rate [37]

3.3.2 Fundamental of crystal growth

The crystal growth process can be divided into four individual steps:

- Adsorption
- Diffusion
- Incorporation
- Desorption

  Once adsorbed the adsorbent have the opportunity to diffuse on the surface and reach a preferable position to incorporate. If incorporation is not possible within a certain time they get desorbed. The steps are discussed briefly in the following section:

- **Adsorption**

  The first step of crystal growth is adsorption. The adsorbent material is often introduced as vapor or as a beam. The amount of material that will stick to the surface depends on the property of the adsorbent and the surface. In VLS mechanism the liquid droplet works like a trap and hence the adsorbent prefers to stick to the droplet and hence the growth rate is enhanced. The curvature of the droplet plays an important role on the adsorption.

- **Diffusion**

  After adsorption the adsorbent is called monomer or adatom and it can diffuse on the surface for a suitable position to incorporate. The diffusion process is totally random. Diffusion plays an important role in the VLS growth of microneedle. The adatom can diffuse on the substrate surface for a certain amount of time and then either desorption or incorporation can take place.

- **Desorption**

  A diffusing monomer always has a possibility to get evaporated i.e. desorbed from the surface. The rate of desorption depends on the temperature, pressure, the surface structure and the monomer characteristics. The desorption rate affects the growth rate in VLS growth method.

- **Incorporation**

  The most important part of crystal growth is incorporation. Diffusion helps the monomers to find suitable place to make a bond and thus to incorporate to the lattice. The monomer lowers its energy by making bond to the lattice.

3.3.3 Growth rate dependency on Au dot diameter

When the Si precursor gas is supplied for *in situ* doped VLS growth of Si microneedle, silicon atoms are adsorbed into the Au-Si alloy droplet in two ways:

1. Direct adsorption of adsorbent into the droplet
2. Diffusion of adsorbent towards the droplet

The growth rate dependency on Au dot diameter will be analyzed considering the above two factors and then the results will be combined to develop a growth rate model.

3.3.3.1 Considering only Direct adsorption

The observation of the experimental microneedles grown by *in situ* doped VLS method shows that in most of the cases the growth rate of smaller diameter needle is lower (Fig. 3.5). The phenomenon is explained in this section using both Gibbs-Thomson effect and Diffusion effect.

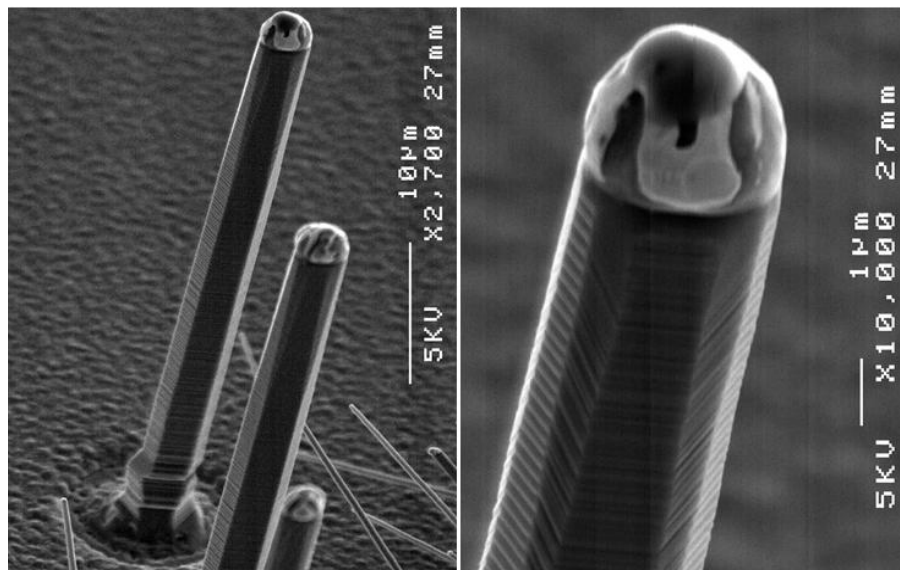

Fig.3.6: Experimentally grown phosphorus doped Si microneedle [37]

To incorporate Gibbs-Thomson effect the shape of the droplet i.e. the diameter and the contact angle need to be examined first. Fig.3.6 shows a close view of an experimentally grown phosphorus doped Si microneedle. It is evident that there is a diameter expansion at the base where it is attached to the substrate.

Givargizov concluded that the "conical expansion at the whisker root is evidently related to a change of the contact angle configuration" [26]. Now it is obvious that the droplet has to undergo some sort of transition in the initial phase of growth, and it is the change of the droplet shape. Fig.3.7 shows the phenomenon.

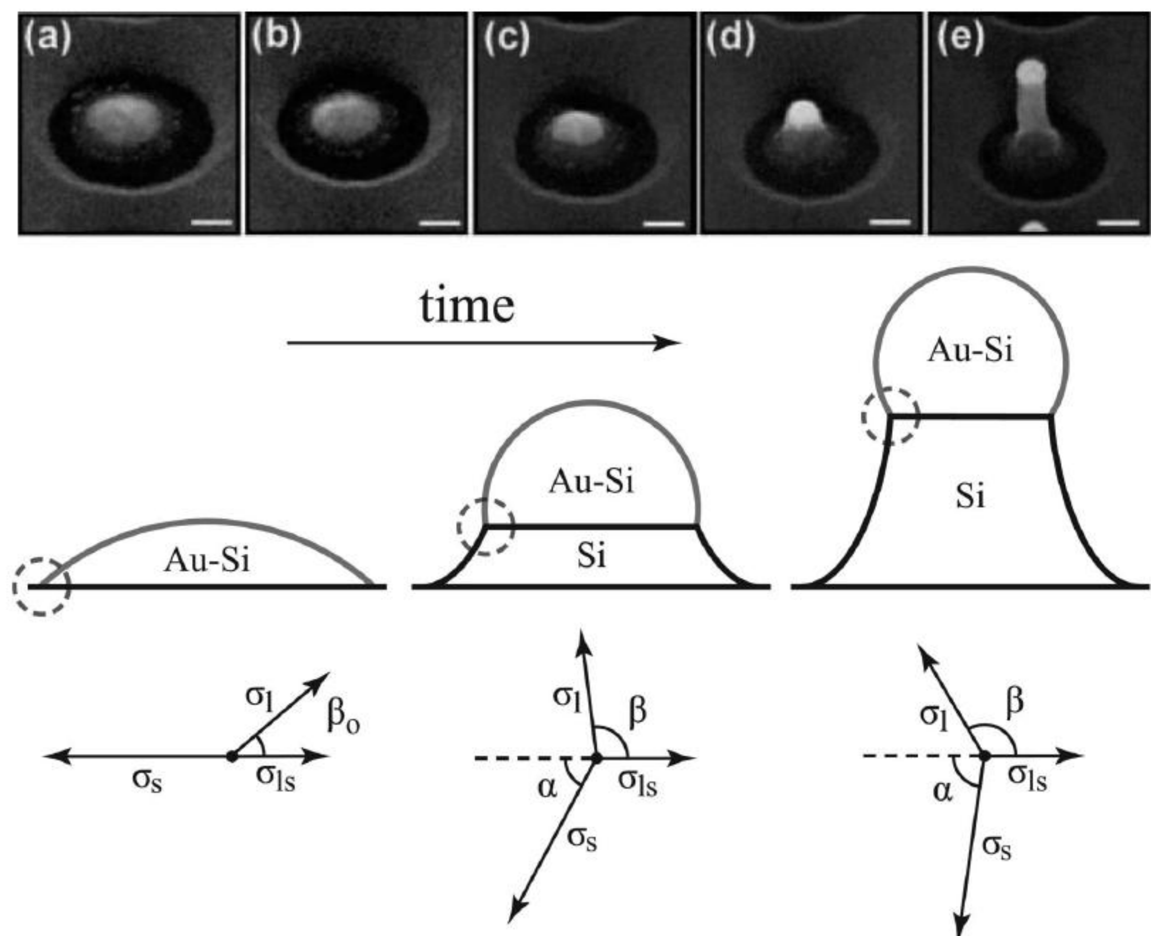

Fig.3.7: Top: Scanning electron micrographs indicating the development of the droplet shape in the initial phase of growth [26]. Center: Schematic development of droplet and wire shape in the initial phase of growth. Bottom: the corresponding equilibrium balance of surface forces at the left edge of the droplet (dashed circles). Note: horizontal force components add up to zero

Now the amount of silicon which is taken by the droplet is proportional to the vapor-droplet interface area and hence the vapor liquid interface area is needed to be derived as a function of contact angle to find out the growth rate. The Au-Si droplets on top of needles are much more spherical, typically exhibiting contact angle of 90-120° [27]. Figure 3.8 shows such spherical droplet with contact angle β>90° and radius "r" on a needle with radius "r_o", which will be used for the derivation.

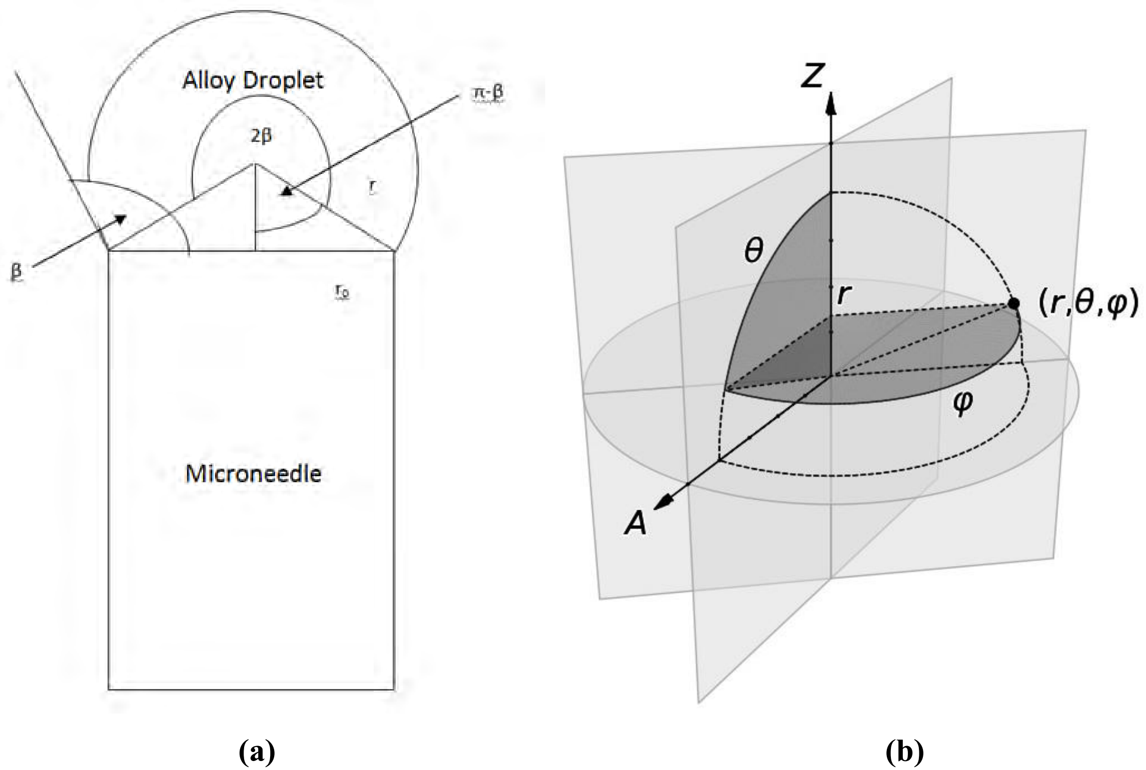

(a) **(b)**

Fig.3.8: (a) Au-Si alloy droplet on Si microneedle (β>90°) (b) spherical coordinate system

The total area of a sphere from spherical coordinate system by integration is as follows:

$$A=\int_0^{2\pi}\int_0^{2\pi} r^2 sin\theta d\theta d\varphi = 4\pi r^2 \quad (3.6)$$

The derivation below is done in case of contact angle β>90° by spherical coordinate system. Area of the alloy droplet (Vapor-liquid interface area)

$=A_{vl}$

$$= \int_0^{2\pi-(2\pi-2\beta)} \int_0^{2\pi} r^2 sin\theta d\theta d\varphi$$

$=r^2 \int_0^{2\pi} [-cos\theta] d\varphi$

$= 2r^2 \int_0^{2\pi} d\varphi$

$=4\beta r^2$

$= \frac{4\beta r_0^{\ 2}}{sin^2\beta}$, where $r_o=rsin\beta$ (3.7)

Again, the amount of Si which is deposited on the liquid solid interface is proportional to the area, which is,

$$A_{ls}=\pi r_0^{\ 2} \quad (3.8)$$

Considering only direct adsorption, the growth rate of Si microneedle will be directly proportional to:

- Chemical potential difference between the vapor phase and liquid phase, $\Delta\mu_d$
- Vapor liquid interface area, A_{vl}

The larger the liquid solid interface area i.e. the diameter of the Au-Si alloy, greater amount of Si atoms will be required for microneedle growth. Hence, the growth rate will be inversely proportional to the liquid solid interface area.

The growth rate of Si microneedle considering only direct adsorption can be expressed as:

$$\text{Growth rate} \propto \frac{\Delta\mu_d(\frac{4\beta r_0^{\ 2}}{\sin^2\beta})}{\pi r_0^{\ 2}} \quad (3.9)$$

$$\text{Or, Growth rate} \propto \left(\Delta\mu_\infty - \frac{4\alpha\nu}{d}\right)\left(\frac{\beta}{\sin^2\beta}\right) \quad (3.10)$$

where, $\Delta\mu_d = \Delta\mu_\infty - \frac{4\alpha v}{d}$ according to Gibbs-Thomson effect.

The Gibbs-Thomson effect can be most easily understood by considering the energetics of a small spherical droplet or particle. The chemical potential μ is the energetic price per atom one has to pay for adding another atom of the same species to the system. For small systems having high surface-to-volume ratios, the influence of the surface on the

thermodynamics cannot be neglected. It is evident that increasing the number of atoms N must necessarily be accompanied by an increase of the surface area and that one has to pay the energetic price for that surface increase as well. For a spherical droplet of radius R and volume $4\pi R^3/3 = N\Omega$, with Ω being the volume per atom (assumed to be constant here), the Gibbs free energy G can be expressed as $G = \mu_\infty N + 4\pi R^2\sigma$, with σ being the surface free energy and μ_∞ being the bulk (infinite radius) chemical potential. By using $\partial R/\partial N = \Omega/(4\pi R^2)$, it can be derived that the chemical potential $\mu = \partial G/\partial N$ is given by $\mu = \mu_\infty + 2\Omega\sigma/R$. This radius dependence of the chemical potential is usually referred to as the Gibbs-Thomson effect. For a cylindrical wire, things are very much the same, but one has to be careful with the quantities that are kept constant and those that are not. The Gibbs free energy of a wire of length L, radius r, and surface free energy σ is given by $G = \mu_\infty N + 2\pi r2\sigma + 2\pi rL\sigma$. Suppose the wire only changes in length; that is, taking the radius to be constant and using $\partial L/\partial N = \Omega/(\pi r^2)$ the chemical potential $\mu = (\partial G/ \partial N)_r$ becomes:

$$\Delta\mu_d = \Delta\mu_\infty - \frac{4\alpha v}{d} \tag{3.11}$$

Where $\Delta\mu_d$ is the gain in chemical potential

$\Delta\mu_\infty$ is the gain of chemical potential for a flat surface

α is vapor-liquid surface energy

ν is the volume of adsorbent atom and d is the diameter of the droplet.

The driving force for the crystal growth is $\Delta\mu_d$, which is called supersaturation and defined as the difference in chemical potential between vapor phase and the solid. The larger the difference between the chemical potentials ($\Delta\mu_d$), the greater is the tendency of phase change from vapor to liquid.

Thus the growth rate equation considering only direct adsorption of adatoms is as follows:

$$\text{Growth rate} \propto \left(\Delta\mu_\infty - \frac{4\alpha v}{d}\right)\left(\frac{\beta}{\sin^2\beta}\right) \tag{3.12}$$

From the above equation it can be stated that:

- Small diameter decreases the driving forces ($\Delta\mu_d$) and hence the microneedle growth rate is slower.
- The contact angle, β remains almost constant as the change in volume involved here is very small, hence the term ($\beta/\sin^2\beta$).

- Therefore, the growth rate is directly proportional to the radius (diameter) of the microneedle i.e. thicker microneedles will have greater growth rate.

Givargizov also reported such kind of growth characteristics [26]. However, this explanation is not fully appropriate in all cases as it only explains the diameter dependency of growth rate of only pure intrinsic microneedles. If doping is introduced i.e. group III/V materials are used as impurity then the behavior could be different [28]. This is described in the following section.

3.3.3.2 Considering only diffusion of adsorbent

Considering diffusion of adsorbent, the growth rate can be derived in two ways:

1) From mass transport model:

J. Johansson *et al* [28] presented a mass transport model based on surface diffusion for nanowire growth and observed that for group III/V materials thinner nanowires are longer than thicker nanowires (Fig. 3.9).

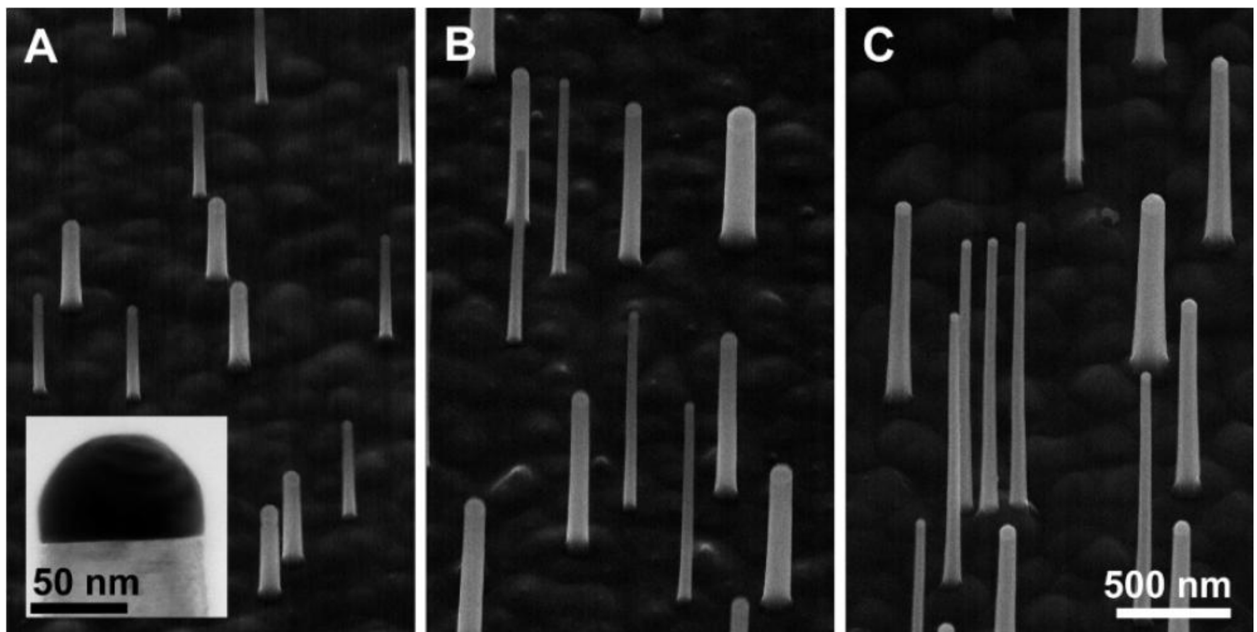

Fig.3.9: Scanning electron micrographs of GaP nanowires grown with MOVPE at different temperatures: (A) 440°C (B) 470°C and (C) 500°C [28]

They demonstrated that the Gibbs-Thomson effect can be neglected in such case. According to the model there is steady state adatom diffusion on the substrate and nanowire sidewalls towards the metal catalyst and the growth rate depends on the following three factors:

1. The diffusion of material directly deposited on nanowire sidewalls.
2. The adatom diffusion from substrate surface up along the nanowire.
3. The material directly deposited on the droplet.

The growth rate equation of the mass transport model is as follows:

$$\frac{dL}{dt} = 2R(1 + \frac{\lambda_W}{r_W}) \quad (3.13)$$

Where L is the length of the nanowire.

R is the deposition rate on the nanowire side and on the droplet.

λ_W represents the diffusion length along the side of the nanowire.

r_W is the radius of the naowire.

The equation is valid for L>> λ_W. From the above equation it is clear that the growth rate for needles with large diameter are lower than the needles with smaller diameter.

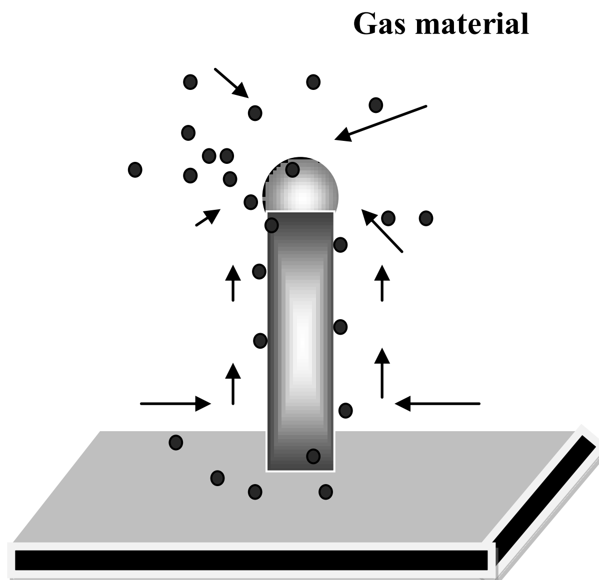

Fig.3.10: Contribution of diffusion in needle growth

2) However, if the diffusion of growth material on the needle surface is considered, the result will be different. If the areal density of Si adatoms diffusing toward catalyst droplet is taken to be constant then the amount of Si per unit time reaching the droplet is proportional to the circumference of the needle ($2\pi r_o$). Moreover, at a given Si supply rate, the growth rate has to be inversely proportional to the needle cross-sectional area (πr_o^2). Combining both, it becomes immediately clear that the growth rate should be inversely proportional to the needle diameter.

$$\text{Therefore, Growth rate } \propto \frac{2\pi r_0}{\pi {r_0}^2} \quad (3.14)$$

$$\text{or, Growth rate } \propto \frac{1}{r_0} \quad (3.15)$$

3.3.3.3 Combining both effects

Now considering both the reason, i.e. the direct adsorption into the droplet and diffusion, the growth rate equation of VLS mechanism becomes:

$$\text{Growth rate} = k_1\left(\Delta\mu_\infty - \frac{4\alpha v}{d} \right) \left(\frac{\beta}{\sin^2\beta}\right) + k_2 \frac{2}{d} \quad \text{, where } r_0 = \frac{d}{2} \quad (3.16)$$

Where k_1 and k_2 are constants. k_1 and k_2 are process parameters which can be obtained by experimental methods.

3.4 Conclusion

In this chapter, growth rate analysis depending on doping level and Au dot diameter is presented. Related physics is used to explain the dependency and growth rate models are proposed It is very important to understand the growth rate dependency on growth conditions in order to control the length and diameter of the *in situ* VLS grown Si microneedles. Using the growth rate models proposed in this chapter it will be possible to anticipate the length of similar phosphorus doped Si microneedle for many applications.

CHAPTER 4

DIAMETER ANALYSIS

4.1 Introduction

In VLS mechanism, it is obvious that the diameter of the microneedle depends on the size of the Au-Si droplet. More specifically, the needle diameter depends on the liquid-solid interface area. To analyze the diameter dependency it is important to understand the behavior of the droplet and a theory of liquid droplet on solid surface is discussed in this chapter. Again it was also observed in this work from experimental data that the doping of phosphorus makes the diameter unstable which is also analyzed later.

4.2 Effect of Au dot size on microneedle diameter

In the experiment cylindrical Au dot of certain Au film thickness and different diameters were used to grow microneedles having various diameters. It is evident that larger droplet and the grown microneedles will have larger diameter.

A theoretical relationship between the Au dot size and the microneedle diameter is derived in this work which is compared with the experimental findings.

4.2.1 Experimental findings

Experimental data shows that if the Au dot diameter is increased keeping the Au film thickness constant, for a fixed doping level the microneedle diameter also increases. The results for different doping level are depicted in Fig.4.1 (a) and (b).

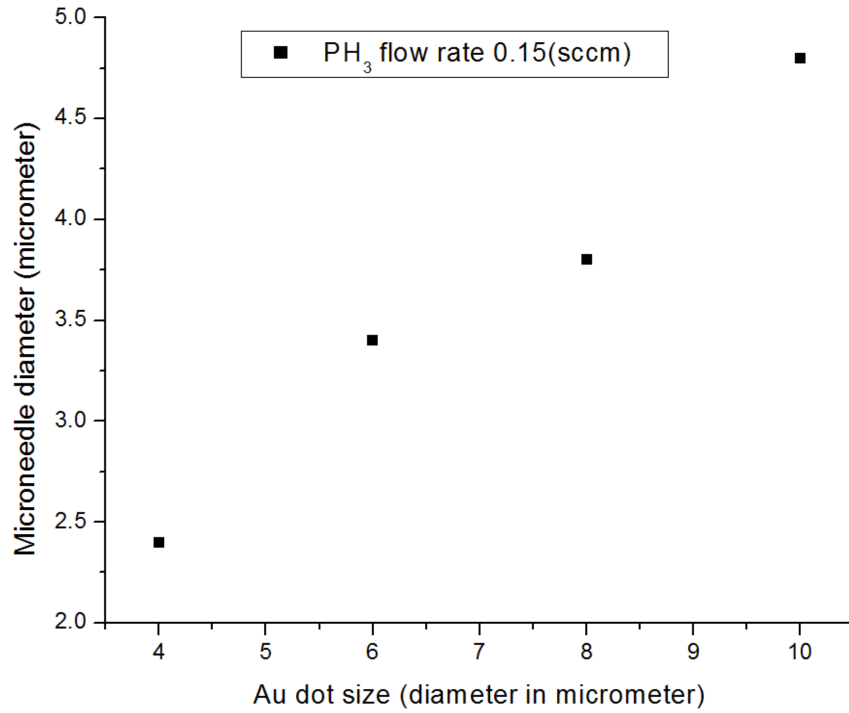

(a)

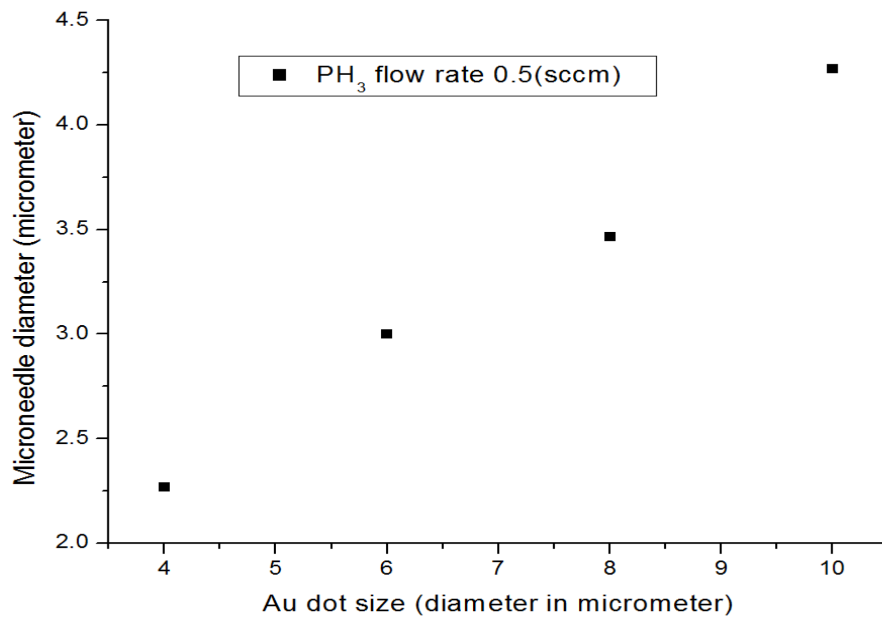

(b)

Fig.4.1: Experimental results of microneedle diameter as a function of Au dot size for PH_3 flow rate (a) 0.15sccm (b) 0.5sccm [37]

The Fig.4.1 above shows that the relationship between microneedle diameter and the Au dot diameter is increasing but not linear. The data table of microneedle diameter for different Au dot size is given in Table 4.1:

Table 4.1: Microneedle diameter for different Au dot size [37]

PH_3 Flow rate 0.15 (sccm)		PH_3 Flow rate 0.5 (sccm)		PH_3 Flow rate 1.0 (sccm)		PH_3 Flow rate 1.7 (sccm)	
Au Dot Diameter (µm)	**Needle Diameter (µm)**	**Au Dot Diameter (µm)**	**Needle Diameter (µm)**	**Au Dot Diameter (µm)**	**Needle Diameter (µm)**	**Au Dot Diameter (µm)**	**Needle Diameter (µm)**
4	2.4	4	2.267	4	2.267	4	2.533
6	3.4	6	3.0	6	3.133	6	2.83
8	3.8	8	3.467	8	3.533	8	3.467
10	4.8	10	4.267	10	4.467	10	-

4.2.2 Theoretical analysis

The shape of the Au dot is like a cylinder as described in the fabrication process in section 2.5.1. Au-Si alloy forms when the Au dot is heated on the Si substrate surface at temperature higher than the eutectic temperature. The alloying process is explained in detail 2.4.3.1. The percent of silicon mix with the gold depends on the temperature and the percent can be measured from the Au-Si binary phase diagram (Fig.2.11). So it can be said that the volume of the Au-Si droplet is proportional to the Au dot volume. From this relation between Au dot diameter and the microneedle diameter can be found.

4.2.3 Mathematical relation

To derive the relation the following assumptions are made:

- The Au dot is cylindrical in nature.
- Radial transverse growth of microneedle diameter due to Vapor Solid (VS) is negligible.
- The microneedle diameter is constant during growth process (neglecting the effect of Au loss)

The contact angle of the droplet on the top of the microneedle is greater than 90° which is shown in the section 3.3.3 and to find out the volume of the droplet we will use Figure 3.10 and the equation of the liquid vapor interface area A_{vl} as derived in section 3.3.3 of chapter three of the book. Thus the volume of the spherical droplet with a contact angle $\beta>90^o$ and radius "r" on a needle with radius "r_o" can be derived as follows:

Volume of the alloy droplet $V_{Au\text{-}Si}=$

$$= \int_0^r A(r)dr$$

$$= \int_0^r 4\beta r^2$$

$$= \frac{4}{3}\beta r^3$$

$$= \frac{\frac{4}{3}\beta {r_0}^3}{sin^3\beta} \quad \text{, where } r_o=rsin\beta \qquad (4.1)$$

Now, the volume of a cylindrical Au dot with diameter "x" and height "h" is:

$V_{Au}= \pi(x/2)^2h$

Now, as the volume of the Au-Si droplet is proportional to the Au dot volume-

$$\frac{\frac{4}{3}\beta {r_0}^3}{sin^3\beta} \propto \pi(x/2)^2h \qquad (4.2)$$

If the contact angle "β" and Au dot height "h" is constant, the relation will be:

$d_o^3 \propto x^2$ where, $d_o= 2r_o$ is the diameter of the needle

or, $d_o \propto x^{2/3}$

or, $d_o =kx^{2/3}$ where, k is a constant (4.3)

Now if we draw the curve from above relationship for an arbitrary value of k= 1.0 the relationship approximately matches the experimental findings (Fig.4.1(a)):

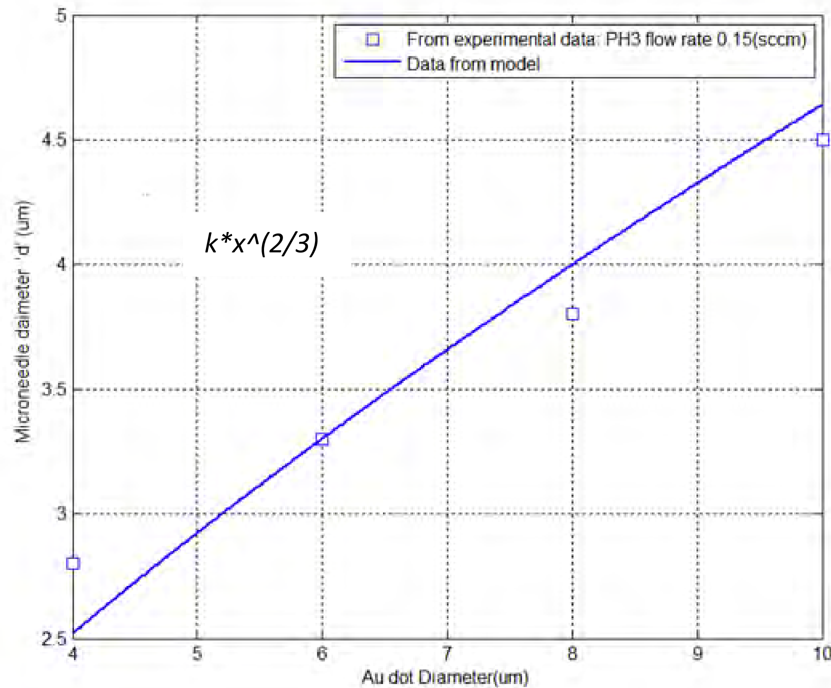

Fig.4.2: Theoretical relation between Microneedle diameter and Au dot diameter

It can be seen from Fig.4.2 that *k* is the determining factor for the microneedle diameter. It is a process parameter which could be obtained by experimental methods for specific growth conditions.

4.3 Effect of doping on microneedle diameter

It has already been reported and explained in previous section that phosphorus doping has severe affect on the growth rate of the microneedle [17] and here the effect of doping on microneedle diameter will be analyzed based on the experimental findings. The incorporation of phosphorus has an effect on surface roughness and the blocking tendency of phosphorus atoms causes a decrease in Si adsorption. These will automatically change the property and shape of the Au-Si alloy droplet and thus affect the diameter of the microneedle.

4.3.1 Experimental findings

Experimental results shows that for a certain Au dot size if doping level is increased the diameter of the microneedle deviates about 0.2µm-0.3µm and seems to have a periodic relation with the doping. The Graph and corresponding data table is given below:

Table 4.2: Experimental data for microneedle diameter for doping level [37]

Au Dot Diameter (4 µm)		Au Dot Diameter (6 µm)		Au Dot Diameter (8 µm)		Au Dot Diameter (10 µm)	
PH_3 Flow Rate (sccm)	Needle Diameter (µm)	PH_3 Flow Rate (sccm)	Needle Diameter (µm)	PH_3 Flow Rate (sccm)	Needle Diameter (µm)	PH_3 Flow Rate (sccm)	Needle Diameter (µm)
0.15	2.8	0.15	3.4	0.15	3.8	0.15	4.8
0.5	2.267	0.5	3.0	0.5	3.467	0.5	4.426
1.0	2.533	1.0	3.067	1.0	3.467	1.0	4.467
1.7	2.533	1.7	2.83	1.7	3.467	1.7	-

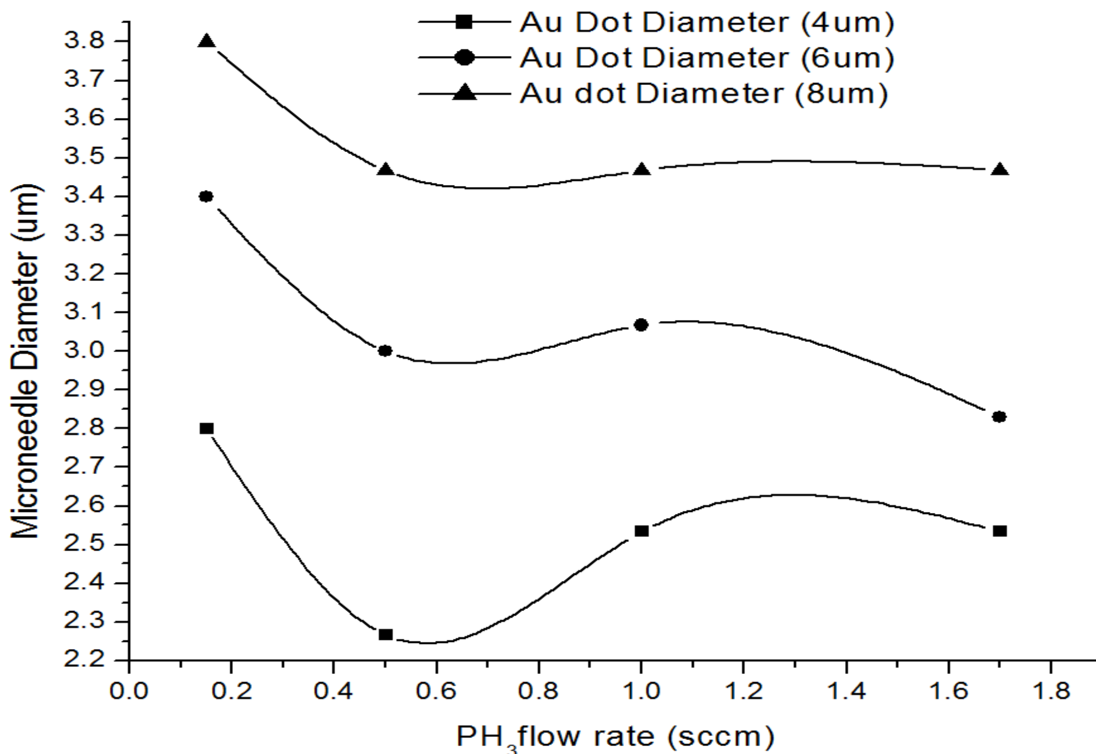

Fig.4.3: Microneedle diameter vs. doping level [37]

4.3.2 Theoretical analysis

The diameter of the microneedle is determined by the liquid solid interface area and hence it is important to find out the initial spreading of Au-Si alloy droplet on the substrate. Au-Si alloy droplets on flat Si substrates and at temperatures of 400-650°C show a contact angle (defined here as the angle within the liquid) of about ≈ 43° [18]. As the experiment of this work was done at 700°C we can assume an initial contact angle of the alloy (inside) $\beta<90^{o}$. B. Ressel *et al* also reported such result of contact angle which is shown in Fig.4.4 [18]. This low value of contact angle indicates a strong liquid-solid interaction and means that the liquid droplet tends to spread on the solid substrate.

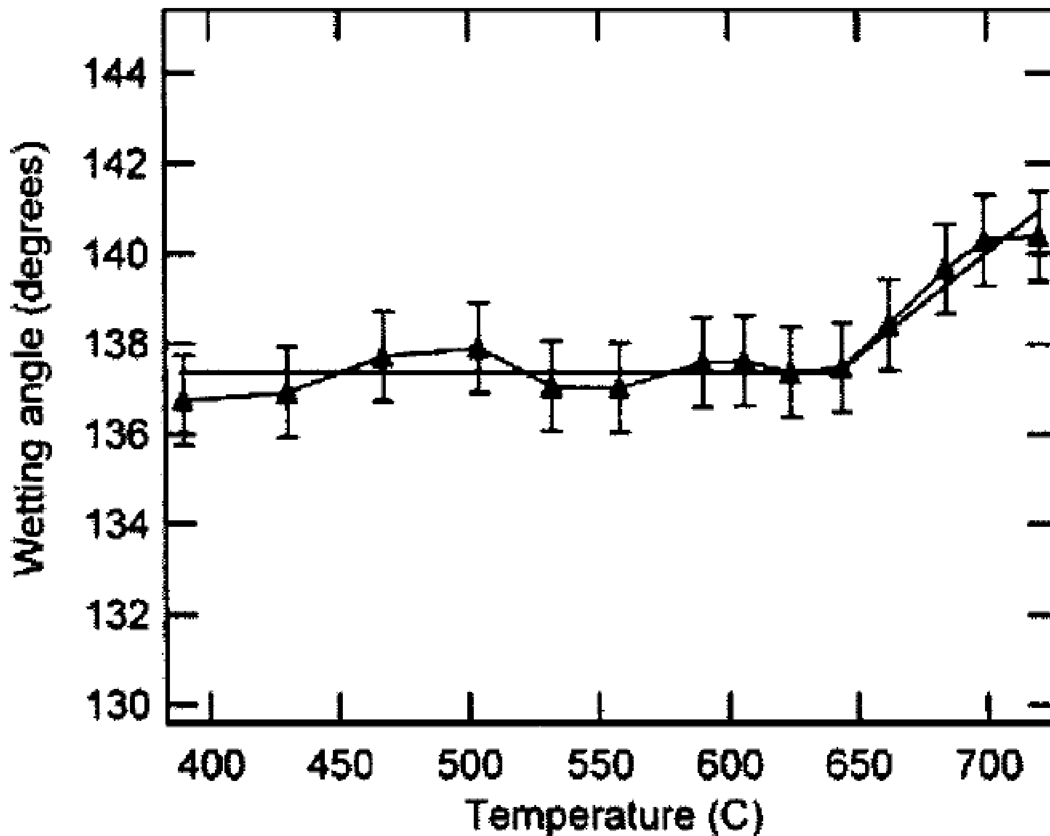

Fig.4.4: Contact angle (measured in gas phase) as a function of temperature [18]

T. Young was the first to describe contact angle equilibrium. The vector summation of forces at the three phase intersection point gives the Young's equation:

$$\gamma_{SV} = \gamma_{SL} + \gamma_{LV} \cos\beta \tag{4.4}$$

Where, γ is the surface tension (or surface free energy)

γ_{SV} *is* the interfacial tensions between solid and vapor.

γ_{SL} *is* the interfacial tensions between solid and liquid.

γ_{LV} *is* the interfacial tensions between liquid and vapor.

The figure of a droplet equilibrium is shown in Fig.4.5. Now the surface roughness depends on the mole fraction of Si in the droplet [18]. If the mole fraction increases the surface roughness also increases.

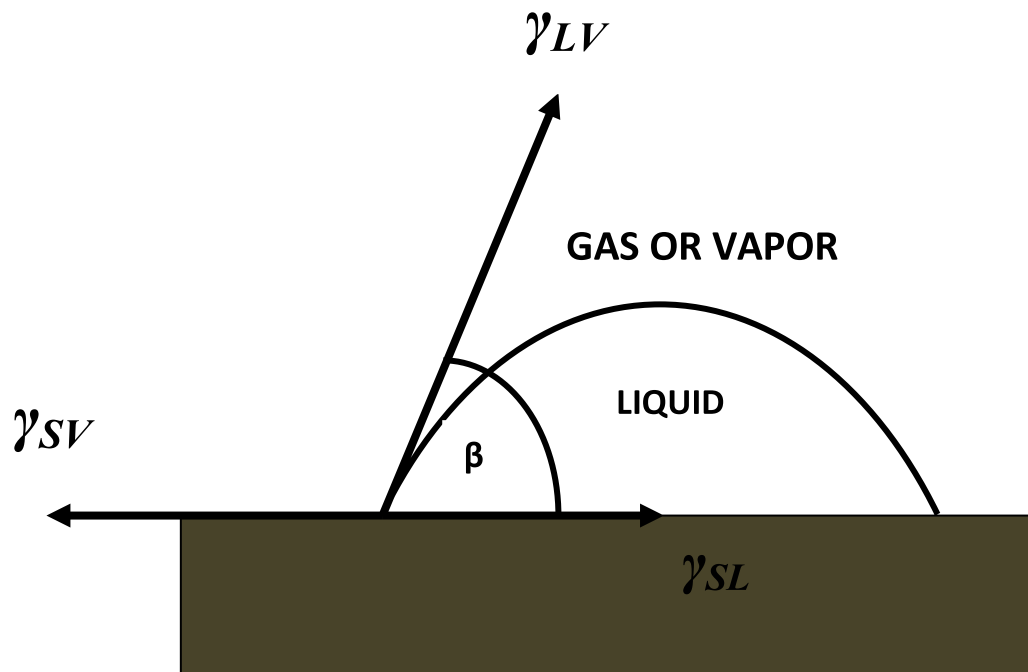

Fig.4.5: Vectorial equilibrium for a droplet of a liquid resting on a solid

The roughness of the liquid-solid interface affects the interface tension at the liquid-solid interface and the vapor-liquid interface. Again if the surface of a substrate is rough, then the actual surface area is greater than the plane (flat) surface area and therefore for a given droplet volume, the total liquid-solid interaction is greater on the rough surface than on a flat surface. If the smooth material gives a contact angle greater than 90°, the presence of surface roughness increases this angle, but if β is less than 90°, the increase in surface roughness decreases the angle which is the case of Au-Si droplet. If the surface roughness 'r_W' is combined with Young's equation the expression of contact angle can be written as [34]:

$$\cos\beta' = r_W \frac{\gamma SV - \gamma SL}{\gamma LV} \quad (4.5)$$

The periodic change in microneedle diameter as a function of doping level now can be explained considering both positive and negative effect: phosphorus doping causes surface roughening as it has strong tendency to segregate [17] and as surface roughness increases, contact angle decreases (Equation 4.4) and the droplet spreads more on the substrate and ultimately the diameter of the miconeedle increases.

Now let us take a look how the negative effect works: Due to the blocking tendency of phosphorus atom, mole fraction of Si atom in the droplet decreases, surface roughness decreases and contact angle increases. As s result the droplet spreads less on the substrate and ultimately the needle diameter decreases. Diameter also decreases if the volume of the droplet decreases due to gold loss.

When the positive effect dominates the negative one, the droplet diameter expansion will cause an increase in the needle diameter and vice versa.

4.4 Conclusion

This chapter provides a detailed analytical study of diameter dependency of phosphorus doped Si microneedle. The diameter of *in situ* doped VLS grown n-Si microneedle more or less increases with increasing Au dot diameter. This phenomenon is supported by the experimental results. The mathematical model proposed to explain the diameter dependency can be used to successfully predict the diameter of n-Si microneedle for

specific growth conditions which might be useful for application of these microneedles in practice. Then the diameter dependency on the doping level is also analyzed along with necessary explanation using related physics which was found to be changing periodically with the increased doping level.

CHAPTER 5
I-V CHARACTERISTICS ANALYSIS

5.1 Introduction

I-V characteristics of phosphorus doped n-type Si microneedles, grown by *in situ* doped VLS mechanism was observed. It was found that the incorporation of doping reduces the resistivity of the needles and shows linear I-V characteristics. Mathematical model of the I-V characteristic is proposed in this chapter which is supported by the experimental values and also the simulation results. This model will be helpful while applying microneedles as sensors for many applications.

5.2 Experimental findings

The current-voltage characteristics of phosphorus doped Si microneedles was measured by using one contact with tungsten (W) microneedle at the tip of the n-Si microneedle and the other tip at the base of the microneedle. For the appropriate placement of the W-needle at the n-Si needle a micromanipulator system was used. Fig.5.1 shows a typical I-V characteristics of microneedle with the length of 52µm and a diameter of 2.8µm grown by VLS method at 720°C and at the growth pressure of 5x10^{-3}Pa for a PH_3 flow rate of 0.15sccm and SiO_2 flow rate of 1.7 sccm. Table 5.1 shows the experimental data:

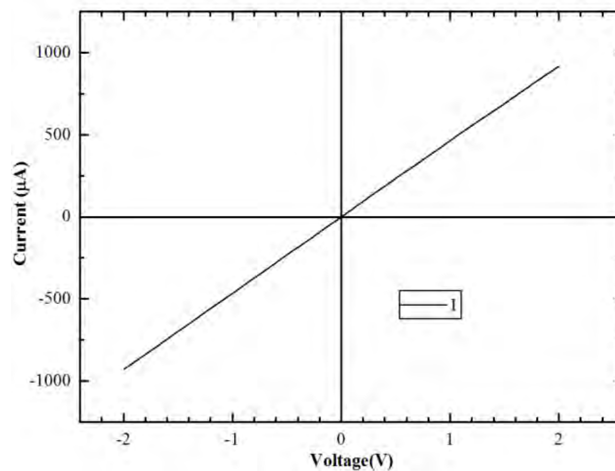

Fig.5.1: I-V characteristics curve of n-Si microneedle with a length of 52µm and a diameter of 2.8µm for PH_3 flow rate of 0.15sccm [37]

Table 5.1: I-V characteristics data of n-Si microneedle with a length of 52µm and a diameter of 2.8µm for PH_3 flow rate of 0.15sccm [37]

Forward Bias V_F (Volt)	Current (A)		Reverse Bias V_R (Volt)	Current (A)
-2	-0.000931		0.1	0.0000467
-1.9	-0.000885		0.2	0.0000933
-1.8	-0.000838		0.3	0.000140
-1.7	-0.000792		0.4	0.000186
-1.6	-0.000745		0.5	0.000233
-1.5	-0.000699		0.6	0.000279
-1.4	-0.000653		0.7	0.000325
-1.3	-0.000606		0.8	0.000371
-1.2	-0.000560		0.9	0.000417
-1.1	-0.000514		1.0	0.000463
-1.0	-0.000467		1.1	0.000509
-0.9	-0.000420		1.2	0.000555
-0.8	-0.000373		1.3	0.000601
-0.7	-0.000327		1.4	0.000646
-0.6	-0.000280		1.5	0.000692
-0.5	-0.000234		1.6	0.000737
-0.4	-0.000187		1.7	0.000782
-0.3	-0.000140		1.8	0.000828
-0.2	-0.000934		1.9	0.000873
-0.1	-0.000467		2.0	0.000918

5.3 I-V analysis

The microneedles grown by Vapor Liquid Solid method are expected to have junctions as gold was used as the catalyst particle and after growth gold remains at the top of the microneedle (Fig.5.2). Current-voltage (I-V) characteristics of phosphorus doped Si microneedle was found linear and exhibits ohmic nature. The microneedles were heavily doped and hence irrespective of the presence of gold particle at the tip the needles exhibits ohmic behavior.

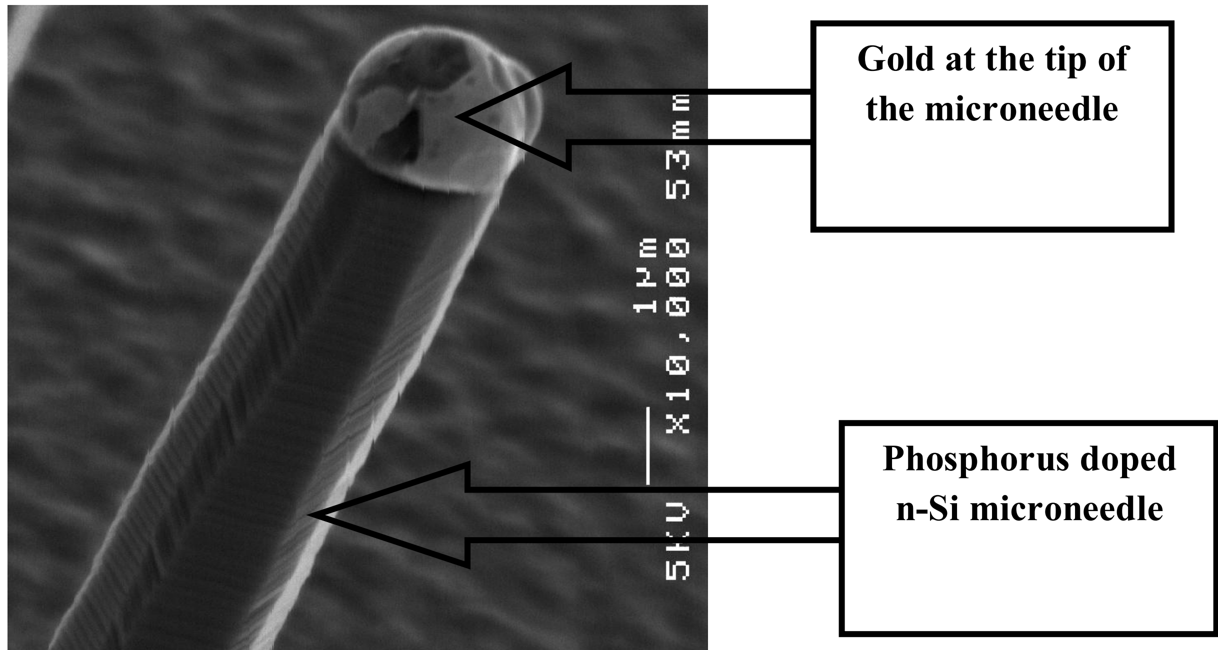

Fig.5.2: SEM image of n-Si microneedle array grown by *in situ* doped VLS [37]

5.3.1 Metal n-type semiconductor contact

In case of ohmic metal-semiconductor contact, charge carriers can flow in either direction without any barrier at interface. However, actually a potential barrier is always found at the junction. The current transport mechanism in such case is essentially quantum mechanical tunneling. The band diagram for the transport though barrier by tunneling is shown in the following Fig.5.3:

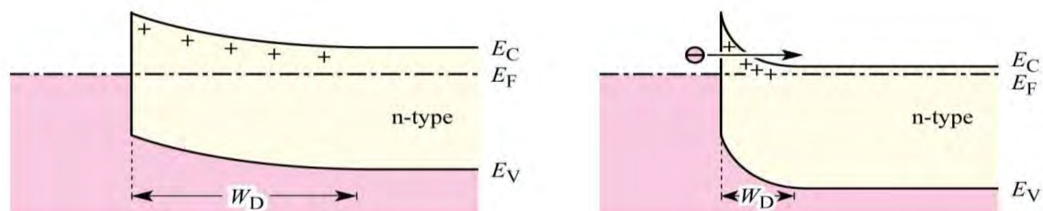

Fig.5.3: Band diagram of metal-n-ype semiconductor ohmic contact

Depending on the doping concentration the I-V characteristics can be very different as the current transport mechanism differs for each situation as shown in the Fig.5.4:

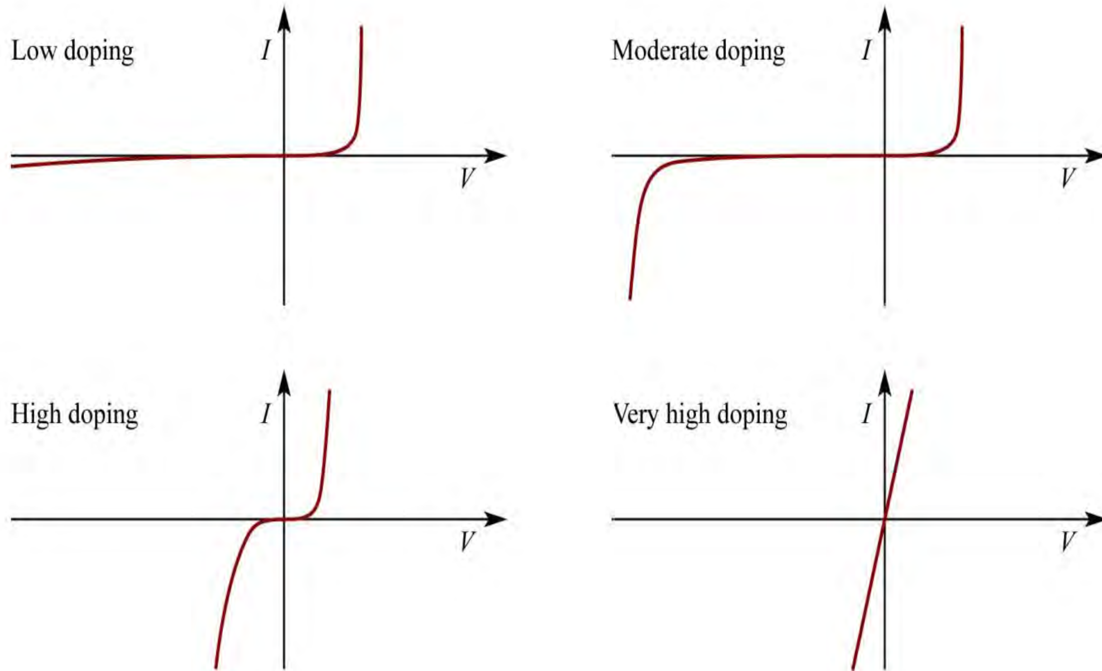

Fig.5.4: I-V characteristics of metal-semiconductor contact for different doping conditions

5.3.2. J-V equation

For more heavily doped semiconductors for operation at low temperatures, the tunneling current becomes more significant. In the extreme of an ohmic contact, which is a metal contact on degenerate semiconductor, the tunneling current is the dominant transport process. The tunneling current from semiconductor to metal $J_{s\rightarrow m}$ is proportional to the quantum transmission coefficient (tunneling probability) multiplied by the occupation probability in the semiconductor and the unoccupied probability in the metal, that is, [31]

$$J_{s\rightarrow m}=\frac{A^{**}T^2}{kT}\int_{E_{Fm}}^{q\varphi_{Bn}} F_s T(E)(1-F_m)dE \qquad (5.1)$$

Where, Fs and F_m are the Fermi-Dirac distribution functions for the semiconductor and the metal respectively, and T(E) is the tunneling probability which depends on the width of the barrier at a particular energy. Theoretical and experimental values of typical current-voltage characteristics for Au-Si barriers are shown in Fig.5.5.

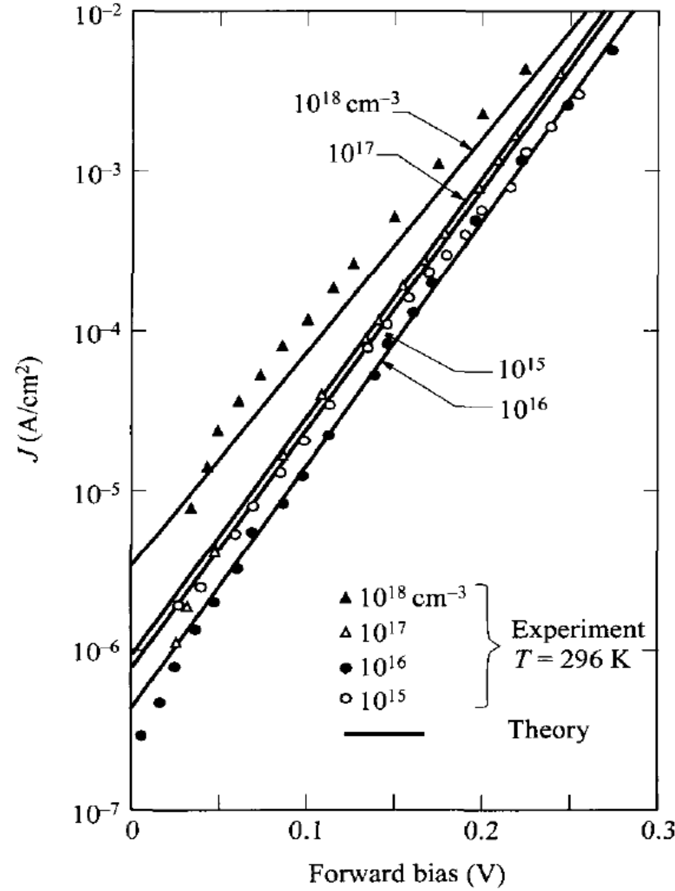

Fig.5.5: Theoretical and experimental current-voltage characteristics for Au-Si Schottky barriers. Increased current is due to tunneling [31]

The *in situ* doped VLS grown microneedles are highly conductive and seem to be highly doped from the I-V characteristics. Hence the dominant current transport process is considered to be quantum mechanical tunneling and thermionic emission process. Considering thermionic emission and tunneling, the J-V relationship is given by Sze [31]:

$$J = J_o\left[exp\left(\frac{qv}{nkT}\right) - 1\right] \quad (5.2)$$

$$J_o = A^{*}T^{2}\, exp\left(-\frac{q\varphi_B}{kT}\right) \quad (5.3)$$

Where, J_o is the saturation current density, $\varphi_B = (\varphi_{Bo} - \Delta\varphi_o)$ is the effective barrier height at zero bias. A^* is the effective Richardson constant given by, $A^* = (4\pi m^* qk^3/H^3)$. The value

of A^* is independent of temperature (Crowell and Sze, 1966) [35]. The effective barrier height at zero bias is given by:

$$\varphi_B = \frac{kT}{q} \ln\left(\frac{A_d A^* T^2}{I_o}\right) \tag{5.4}$$

Where A_d is the Schottky contact area, I_o is the saturation current at zero bias, the ideality factor η is given by:

$$\frac{1}{\eta} = \frac{kT}{q}\frac{d}{dV} ln\left[\frac{J}{\{1-\exp(-qV/kT)\}}\right] \tag{5.5}$$

For V> 3qT,

$$\frac{1}{\eta} = \frac{kT}{q}\frac{d(lnJ)}{dV} \tag{5.6}$$

In the reverse direction, the J-V relation is as follows:

$$J_R \approx A^{**}T^2 \exp\left(\frac{q(\varphi_{Bo} - \sqrt{q\xi_m/4\pi\varepsilon_s})}{kT}\right) \tag{5.7}$$

Where, A^{**} is the modified Richardson constant considering the impact of electron emission and tunneling, ξ_m is the maximum electric field at metal-semiconductor interface and ε_s is the semiconductor permittivity. As no diffused guard ring was introduced during fabrication, the sharp edge effect must be present and hence the dominant reverse bias current is due to the edge leakage. Due to the quantum mechanical effect some electron from gold penetrates into the silicon energy band and results in a static dipole layer at the Au-Si contact surface. This dipole layer is responsible for varying barrier height slightly with the field in the reverse bias. The static voltage lowering is expressed as follows:

$$\Delta\varphi_{static} \approx \alpha\xi_m \tag{5.8}$$

5.3.3 Simulation result

A needle shaped phosphorus doped n-Si microneedle with gold at the top as a cathode was simulated for I-V analysis. The length and diameter of the needle was 52µm and 2.9µm respectively. The first simulation was done for low doping i.e. for doping concentration $1.39 x 10^{14} cm^{-3}$. The second simulation was done assuming that the Au-Si contact is working as an Ohmic contact. At room temperature (300K) with uniformly phosphorus doped needle with doping concentration $1.39 x 10^{17}$ cm^{-3} shows almost same I-V characteristics as found experimentally. The I-V characteristics curve from simulation is shown in Fig.5.6 and Fig.5.7. The simulation is done for Ohmic contact and the doping is chosen to be uniform for simulation.

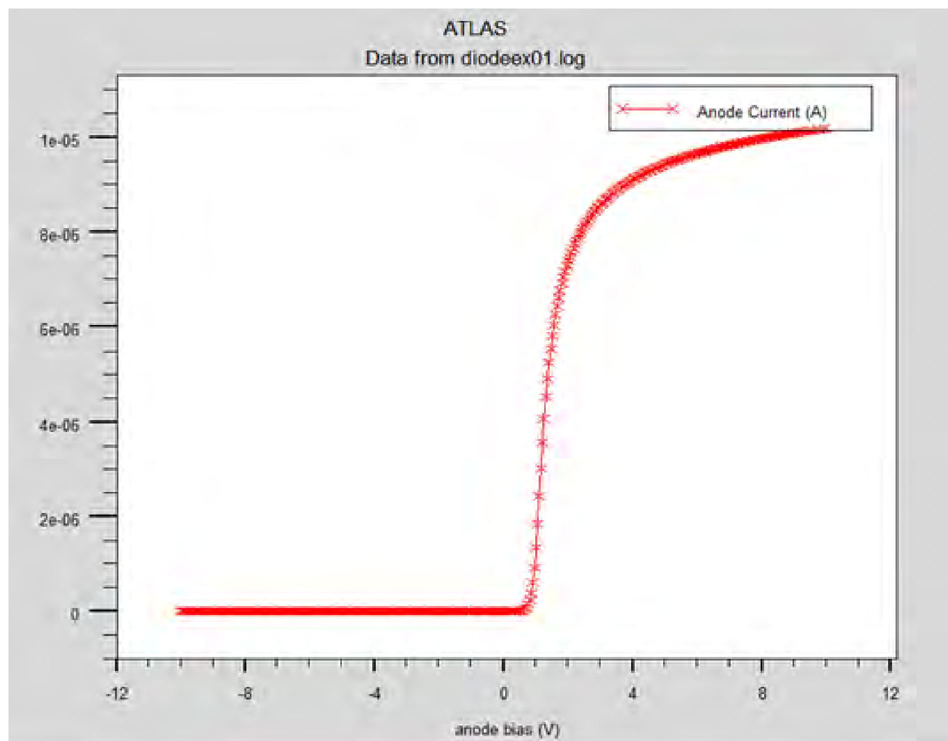

Fig.5.6: I-V characteristics curve of n-Si microneedle from Atlas simulator (for low doping level)

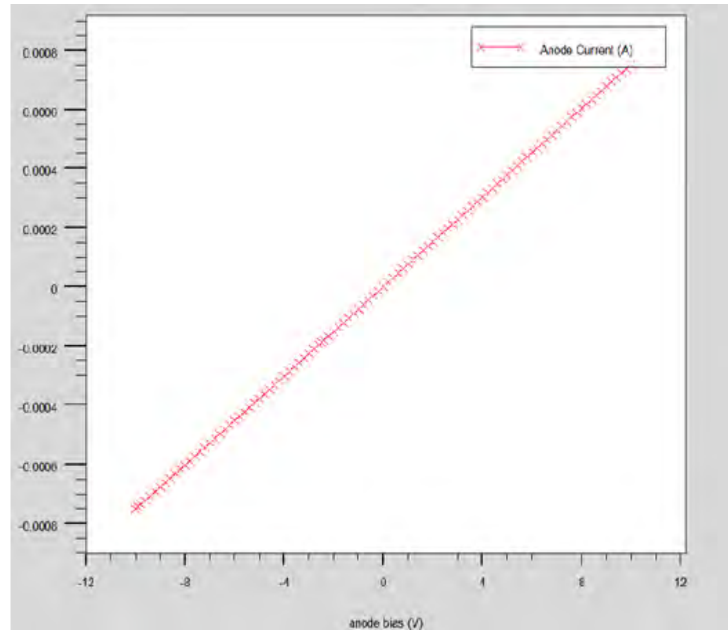

Fig.5.7: I-V characteristics curve of n-Si microneedle from Atlas simulator (for high doping level)

5.3.4 Comparison between experimental and simulation result

From the comparison between the simulated and experimental results it is seen that there is some difference between them as shown in Fig.5.8:

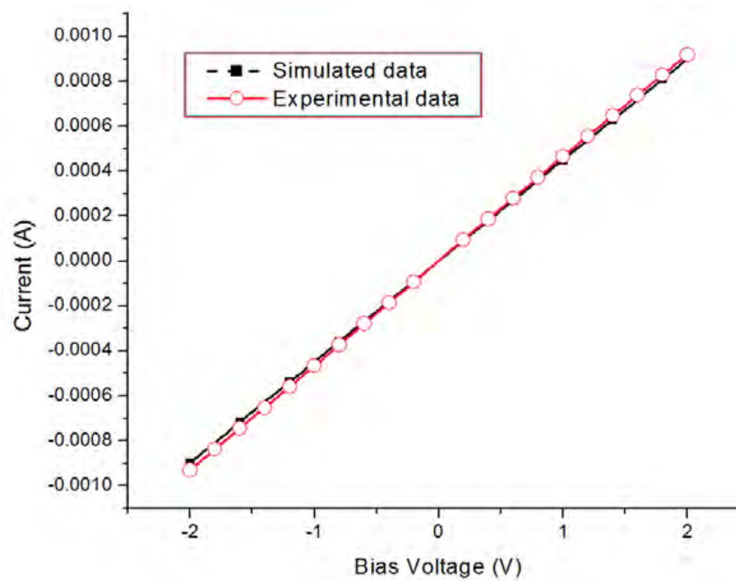

Fig.5.8: I-V comparison between the simulated data and experimental data

The following Table 5.2 shows the comparison between the results of simulation and experimental data:

Table 5.2: Table comparing Experimental and simulated data for I-V characteristic

Bias Voltage (Voltage)	Experimental Data Current, I (A)	Simulated Data Current, I (A)
-2.0	-0.000931	-0.000897819
-1.8	-0.000838	-0.000808039
-1.6	-0.000745	-0.000718259
-1.4	-0.000653	-0.000628478
-1.2	-0.000560	-0.000538696
-1.0	-0.000467	-0.000448914
-0.8	-0.000373	-0.000359132
-0.6	-0.0002.80	-0.000269349
-0.4	-0.000187	-0.000179566
-0.2	-0.0000934	-0.0000898
0.2	0.0000933	0.0000898
0.4	0.000186	0.000179566
0.6	0.000279	0.000269349
0.8	0.000371	0.000359132
1.0	0.000463	0.000448915
1.2	0.000555	0.000538696
1.4	0.000646	0.000628478
1.6	0.000737	0.000718259
1.8	0.000828	0.000808039
2.0	0.000918	0.000897819

5.4 Conclusion

In this chapter, the electrical property of n-Si microneedle is analyzed. This analysis clearly shows that the doping level changes the electrical properties of the n-Si microneedle which is evident from both simulation result and experimental result. This criterian can be used to fabricate microneedles of desired electrical properties.

CHAPTER 6
CONCLUSION AND FUTURE WORK

6.1 Summary

This thesis work has been devoted to the development of analytical models of growth rate and diameter of n-Si microneedle depending on two growth conditions i.e. the doping level and Au dot diameter. Mystery related to physical and electrical properties of phosphorus doped Si microneedle grown by *in situ* doped VLS method are unfolded in this research work.

Chapter 3 of this thesis includes detailed growth rate analysis. The growth rate analysis was twofold. First of all, the growth rate dependency on doping level was analyzed along with necessary explanation. Related physics was used to develop the analytical model for growth rate. Phosphorus doping into *in situ* doping VLS results in the reduction of growth rate which has been incorporated to the blocking tendency of phosphorus atoms. These atoms block active surface sites for adsorption of Si atoms and thus the instantaneous growth is inhibited as Si could only be adsorbed on the Si sites. This phenomenon is also modeled analytically and the results obtained for a set of growth conditions were compared to those of the experimental results. Secondly, the growth rate dependency on Au dot diameter was also analyzed and analytical model was developed considering direct adsorption and diffusion of Si atoms into the Au-Si alloy droplet. Gibbs-Thomson effect and diffusion effect were considered used for the derivation of the analytical model.

In chapter 4, the diameter analysis was carried depending on doping level and Au dot diameter. The dependency on Au dot size was successfully modeled and the result derived from the model was compared to the experimental result. The diameter of the VLS grown needle was found to be increasing with increasing Au dot diameter. Diameter of the microneedle also depends on the doping level. This dependency is periodic and the dependence was explained using Young's surface tension equilibrium equation. Surface roughness and contact angle of the microneedles play a vital role in determining the

diameter of the needle and therefore these factors were incorporated in the Young's equation.

The growth rate and diameter model and theoretical analysis in this thesis will be very helpful to anticipate the size (length and diameter) of such n-type microneedles and hence to fabricate microneedles of desired length and diameter for many applications.

Moreover, the electrical property of the microneedles and the I-V characteristics is analyzed in chapter 5. The phosphorus doped silicon microneedles grown by VLS mechanism shows I-V characteristics similar to that on an Ohmic contact which can be very helpful in sensor applications. Therefore, it is vital to obtain a better understanding of the basic electrical properties of the metal-semiconductor interface of the microneedles. The Si microneedles have greater mechanical strength than those of Si nanowires and hence suitable for using as inserting needle to collect neural signals and for drug delivery. Doped silicon needles are more conductive and therefore they are appropriate to collect small signals from living cells. However as doping changes the I-V characteristics of microneedles in VLS mechanism, the complete electrical analysis supported by simulation in this thesis work will also be helpful to improve the I-V characteristics in future while fabricating vertical devices like diodes, transistors with microneedles.

6.2 Scope of future research work

Silicon is utilized in a vast range of electrical devices as it has well-established electronic and excellent mechanical properties. Application of Si micro/nanostructures in applications like sensors and transducers require extensive research. There are many directions in which this research can be extended. Some of the ideas are discussed in this section:

- These structures have great prospect to be used as pressure sensors. For such uses the phosphorus doped silicon microneedle should be studied extensively so that the mechanical properties like elastic modulus and hardness could be measured. The mechanical properties of such n-type microneedles are still unexplored and it offers a prospective area of research.
- Si microneedles have excellent optical properties and a few applications have been reported [36] but there is lack of theoretical analysis of optical

properties of Si microneedle. Application of Si microneedles as photo sensors or optical neurostimulator and study of their physical and optical properties can be a great avenue for research.

- It is observed from the experimental data that the Si needles are tapered with a certain slope. It might be due to the radial growth. Theoretical detailed study and modeling of the radial growth is of utmost importance.
- The effect of changing temperature and pressure on the growth dynamics of Si microneedles was out of scope of this research work. This work can be extended considering the effect of temperature and pressure.

REFERENCES:

[1] S. Asai , K. Kato, N. Nakazaki, and N. Nakajima, "Probe card with probe pins grown by the vapor-liquid-solid (VLS) method," *IEEE Trans. Component, Packaging, and Manufacturing Tech.-Part A*, Vol. 19, no. 2, pp. 258-267, 1996.

[2] T. Kawano, H. Takao, K. Sawada, and M. Ishida, "Multichannel 5X5-site 3-dimensional Si microprobe electrode array for neural activity recording system," *Jpn. J. Appl. Phys.*, Vol.42, pp. 2473-2477, 2003.

[3] T. Kawano, H. Takao, K. Sawada, and M. Ishida, "Neural recording chip with penetrating Si microprobe electrode array by selective vapor-liquid-solid growth method," *IEMBS 2004*, pp. 2066-2069, September 2004.

[4] K. Takei, T. Kawashima, T. Kawano, H. Takao, K. Sawada, and M. Ishida, "Integration of out-of-plane silicon dioxide microtubes, silicon microprobes and on-chip NMOSFETs by selective vapor–liquid–solid growth," Journal of Micromechanics and Microengineering, Vol. 18, pp. 0350033, 2008.

[5] L. Lin and A.P. Pisano, "Silicon Processed Microneedles," *IEEE Journal of MEMS*, Vol. 8, no. 1, March 1999.

[6] J. Held, J Gaesper, P. J. Koester, C. Tautorat, A. Cismak, W. Baumann, A. Trautman, P. Ruther, and O. Paul, "Microneedle arrays for intracellular recording applications," *In: IEEE MEMS Congress Proceedings*, Tuscon, USA, pp. 268-271, 2008.

[7] V. Schmidt, H. Riel, S. Senz, S. Karg, W. Riess, U. Gesele, "Realization of a Silicon Nanowire Vertical Surround-Gate Field-Effect Transistor," *Small 2006*, Vol. 2, pp. 85-88, 2006.

[8] T. Kawano, Y. Kato, M. Futawaga, H. Takao, K. Sawada, and M. Ishida, "Fabrication and properties of ultrasmall Si wire arrays with circuits by vapor-liquid-solid growth," *Sensors and Actuators*, Vol. A 97-98, pp. 709-715, 2002.

[9] T. Kawano, Y. Kato, R. Tani, H. Takao, K. Sawada, and M. Ishida, "Selective Vapor-Liquid-Solid Epitaxial Growth of Micro-Si Probe Electrode Arrays With On-Chip MOSFETs on Si (111) Substrates," *IEEE Trns. Electron Devices*, Vol. 51, pp. 415-420, 2004.

[10] A. Ikedo, M. Ishida, and T. Kawano, "Out-of-plane high-density piezoresistive silicon microwire/p–n diode array for force- and temperature-sensitive artificial whisker sensors," *Journal of Micromechanics and Microengineering*, Vol. 21, pp. 035007 (7pp), 2011.

[11] Adele C. T., Christopher T. C., Emily L. W., Daniel B. T., Michael D. K., Nathan S. L., and Harry A. A., “Wafer-Scale Growth of Silicon Microwire Arrays for Photovoltaics and Solar Fuel Generation,” IEEE Journal of Photovoltaics, Vol. 2, Issue. 3, pp. 294-297, July 2012.

[12] R. S. Wagner, and W. C. Ellis, “Vapor-liquid-solid mechanism of single crystal growth,” *Applied Physics Letters*, Vol. 4, pp.89-90, 1964.

[13] M. S. Islam, K. Sawada, M. Ishida, “VLS growth of Doped Si-microprobe arrays using varying PH_3 flow with fixed flow of Si_2H_6 at low temperature,” *In: IEEE 5th International Conference on Electrical and Computer Engineering*, Dhaka, Bangladesh, pp. 251-254, 2008.

[14] B. Stoeber and D. Liepmann, “Arrays of Hollow Out-of-Plane Microneedles for Drug Delivery,” *Journal of Microelectromechanical System*, Vol. 14, no. 3, pp. 472-479, June 2005.

[15] M. S. Islam, T. Kawashima, K. Sawada, and M. Ishida, “Realization of *In Situ* Doped n-type and p-type Si-Microprobe Array by Selective Vapor-Liquid-Solid (VLS) Growth Method ,” *Journal of Crystal Growth*, Vol.306, pp. 2161-2165, 2005.

[16] M. S. Islam, T. Kawashima, K. Sawada, and M. Ishida, “High-yield growth of p-Si microprobe arrays by selective vapor-liquid-solid method using in-situ doping and their properties,” *Journal of Crystal Growth*, Vol.306, pp.276-282, August 2007.

[17] Gao, F., Huang, D. D., Li, J. P, Lin, Y. X, Kong, M. Y., Sun, D. Z., Li, J. M. and Lin, L. Y., “Influence of phosphine flow rate on Si growth rate in gas source molecular beam epitaxy,” *J. Cryst. Growth*, Vol. 220, pp. 461-465, 2000.

[18] B. Kalache, P. Roca and A. Fontcuberta, “Observation of Incubation Times in the Nucleation of Silicon Nanowires Obtained by the Vapor-Liquid-Solid Method,” *Japanese Journal of Applied Physics*, Vol. 45, No. 7, pp. L190-L193, February 2006.

[19] B. Ressel, K. C. Prince, and S. Heun, “Wetting of Si surfaces by Au-Si liquid alloys,” *Japanese Journal of Applied Physics*, Vol.93, pp. 3886-3892, 2003.

[20] Y. V. Naidich, V. Zhuravlev, N. Krasovskaya, “The wettability of silicon carbide by Au-Si alloys,” *Materials Science and Engineering A245 (1998)*, pp. 293-299, 1998.

[21] H. Kohono, and S. Takeda, “Periodic instability in growth of chains of crystalline-silicon nanospheres,” *Journal of Crystal Growth*, Vol. 216, pp. 185-191, March 2000.

[22] S. M. Sze, "Physics of Semiconductor Devices" 3rd Edition, John Willey and Sons, New York, 2007, p.134-196.

[23] S. A. Moiz, S. W. Jee, H. D. Um, and J. H. Lee, "Electrical Characterization of Metal–Silicon Microwire Interface Using Conductive Atomic Force Microscope," *Japanese Journal of Applied Physics*, Vol.49, pp. 045003, 2010.

[24] Yi Cui, Xiangfeng Duan, Jiangtao Hu, and Charles M. Lieber, " Doping and Electrical Transport in Silicon Nanowires," *Journal of Physical Chemistry*, Vol. 104, pp. 5213-5216, June 2000.

[25] V. Schmidt, J. V. Wittemann, S. Senz, and U. Gosele, "Silicon Nanowires: A Review on Aspects of their Growth and their Electrical Properties," *Advanced Materials*, Vol. 21, Issue. 25-26, pp. 2681-2702, July 13, 2009.

[26] E.I. Givargizov, "Growth of Whiskers by Vapor Liquid Solid Mechanism," *J. Cryst. Growth 1975*, Vol. 1, 31, 20, 1975.

[27] S. Kodambaka, J. Tersoff, M.C. Reuter, F.M. Ross, "Diameter Independent Kinetics in the Vapor-Liquid-Solid Growth of Si Naowires ," *Phys. Rev. Lett.*, Vol. 96, pp. 096105-096109, March 2006.

[28] J. Johansson, C.P.T. Svensson, T. Martensson, L. Samuelson, and W. Seifert, "Mass Transport Model for Semiconductor Nanowire Growth," *Journal of Physical Chemistry*, Vol. 109, pp. 13567-13571, May 2005.

[29] B. Cho, J. Bareno, Y.L. Foo, S. Hong, T. Spilla, I. Petrov, and J.E. Greene, "Phosphorus incorporation during Si(001):P gas-source molecular beam epitaxy: Effects on growth kinetics and surface morphology," *Journal of Applied Physics*, Vol. 103, pp. 123530, 2008.

[30] D. Kashchiev, "Dependence of the Growth rate of Nanowires on the Nanowire Diameter," *Crystal Growth and Design*, Vol. 6, No. 5, pp. 1154-1156, February 2006.

[31] S.M. Sze, "Physics of Semicoductor Devices" 3rd Edition, John Willey and Sons, New York, 2007, pp. 134-196.

[32] S.M. Jang, K. Liao and R. Reif, "Phosphorus doping of epitaxial Si and $Si_{1-x}Ge_x$ at very low pressure," *Appl. Phys. Lett.*, Vol. 63, No. 12, pp. 1675-1677, September 1993.

[33] B.S. Meyerson, M.L.Yu, *Journal of Electrochemical Society*, Vol. 131, pp. 2366, 1984.

[34] H.Y. Erbil, "Surface Chemistry of Solid and Liquid Interfaces," 1st edition, Blackwell Publishing Ltd., UK, 2006, pp. 308-337.

[35] S. M. Sze, "Physics of Semiconductor Devices" 3rd Edition, John Willey and Sons, New York, 2007, p.134-196.

[36] A. C. Tamboli, C. T. Chen, E. L. Warren, D. B. Turner-Evans, M. D. Kelzenberg, Nathan S. Lewis, and H. A. Atwater "Wafer-Scale Growth of Silicon Microwire Arrays for Photovoltaics and Solar Fuel Generation," IEEE *Journal of Photovoltaics*, Vol. 2, Issue 3, pp.294-297, July 2012.

[37] Md. Shofiqul Islam, "Doped n-Si Microprobe Arrays by Vapor Liquid Solid Growth Using *In situ* Doping and Their device application," Thesis: Doctor of Engineering, Toyohashi University of Technology, Japan, April, 2007.